ALTERRA
WAGENINGEN UR

Modelling water temperature in TOXSWA

Alterra Report 2099
ISSN 1566-7197

C.M.J. Jacobs, J.W. Deneer and P.I. Adriaanse

Modelling water temperature in TOXSWA

Commissioned by the the Ministry of Agriculture, Nature and Food Quality
Projectcode: [BO-12-07-002-ALT-6]

Modelling water temperature in TOXSWA

C.M.J. Jacobs, J.W. Deneer, P.I. Adriaanse

Alterra-report 2099

Alterra Wageningen UR
Wageningen, 2010

Abstract

C.M.J. Jacobs, J.W. Deneer and P.I. Adriaanse, 2010. *Modelling water temperature in TOXSWA* Wageningen, Alterra, Alterra-report 2099. 60 p.; 9 fig.; 3 tab.;34 ref.

A reasonably accurate estimate of the water temperature is necessary for a good description of the degradation of plant protection products in water which is used in the surface water model TOXSWA. Based on a consideration of basic physical processes that describe the influence of weather on the energy balance of natural water bodies, we propose to extend TOXSWA with a 1D bulk approach to estimate water temperature. Evaluation of such a system confirmed that it is physically realistic and yet simple, with limited data requirements. It is expected to perform reasonably well in most conditions, and fits well into the present structure of the TOXSWA model. In particular the estimation of degradation rates in shallow and turbid water will benefit from introducing the proposed system.

Keywords: bulk model, decay of plant protection products, water temperature, TOXSWA.

ISSN 1566-7197

The pdf file is free of charge and can be downloaded via the website www.alterra.wur.nl (go to Alterra reports). Alterra does not deliver printed versions of the Alterra reports. Printed versions can be ordered via the external distributor. For ordering have a look at www.boomblad.nl/rapportenservice.

Alterra-report 2099
Wageningen, februari 2010

Contents

Acknowledgement

The authors would like to thank Bert Meijering for allowing the use of the experimental observations in our evaluation of the proposed modelling system. The data from the weather station in De Bilt were obtained from the Royal Netherlands Meteorological Institute (KNMI) in De Bilt (www.knmi.nl).

Summary

The TOXSWA (TOXic substances in Surface WAters) model simulates the concentration of plant protection products (PPP) in small surface waters. The degradation rate of PPP has a large impact on the evolution of PPP concentration. Estimation of the degradation rate of PPP in water is therefore an important component of the TOXSWA model. Processes governing the rate at which PPP disappear are often affected by temperature. Thus, a reasonable estimate of the water temperature is needed in order to get a good description of the degradation of PPP in water.

In the current version of the TOXSWA model the water temperature is estimated in a simplified way, using monthly averages of the air temperature. However, water bodies in the open air are strongly influenced by weather conditions that vary at timescales down to one hour. To get a proper description of the response of water temperature to the weather conditions, calculations need to be based upon the most important physical principles governing the interaction between the atmosphere and the water. Moreover, other processes that affect the water temperature, such as drainage, need to be accounted for as well.

The main goal of the study presented in this report is to provide suggestions for improvement of the TOXSWA estimates for water temperature in small surface waters. The new algorithm should be able to simulate the temperature in small water bodies at hourly to seasonal timescales. It must provide physically realistic estimates, but at the same time be as simple as possible and easy to implement in the existing TOXSWA environment. Data used to drive the model must be readily available.

The processes determining the temperature of a natural water body can be divided into the following categories:

1. Exchange of energy at the air-water interface
2. Absorption of solar radiation in the water
3. Exchange of heat with the sediment and the environment
4. Mixing in the water
5. Supply and extraction of energy through external mechanisms

Categories 1 - 4 are processes that will mostly occur naturally and are suited for a one dimensional (1D) description. The exchange of energy between water and the atmosphere at the air-water interface progresses through transfer of sensible heat, evaporation and condensation, exchange of longwave radiation and heat transfer through precipitation. They are all directly related to the weather conditions. Absorption of solar radiation in the water column is of particular importance, especially in summer time. This process is not only related to the weather conditions, but the turbidity of the water is crucial as well. Exchange of heat between water and sediments and with the surrounding soil usually is small, but in some cases wall effects may have to be considered. Mixing in the water is caused by density effects related to heat exchange, absorption of radiation, and momentum transfer between the water and the air or the sediment and walls. Category 5 is concerned with more or less artificial processes like supply of drainage water as well as natural processes like surface runoff. These mechanisms are considered to be 'external' because they cannot take place through local, natural 1D-exchange.

For many practical applications a 1D bulk model with the assumption of a well-mixed water layer is expected to be sufficiently accurate, provided the most important components of the energy balance are modelled with reasonable accuracy. In particular the fluxes at the air-water interface and the absorption of solar radiation in

the water column have to be modelled in a physically realistic way. Errors in the energy budget arising from the fact that temperature gradients near the surface or at the water-sediment interface are neglected are considered acceptable for most applications. A 1D bulk model can be applied quite easily in a quasi-2D framework. Extension to such a quasi-2D framework relies on the assumption that the control volume is well-mixed horizontally, that is, the control volume is assumed to be horizontally homogeneous. This assumption is already in place in TOXSWA.

It is concluded that for use in TOXSWA it is advisable to design a 1D-bulk model for simulation of the thermal behaviour of water bodies. The main modules required to obtain a reasonably accurate 1D bulk model are described, along with their numerical implementation and guidelines for specification of the initial and boundary conditions.

The proposed modelling system has the following main limitations:
(i) thermal stratification cannot be handled
(ii) the light absorption model will not necessarily be valid for systems where macrophytes dominate light absorption
(iii) the possible influence of walls on radiation exchange is not taken into account
(iv) cases where horizontal exchange is exceptionally large in comparison with the vertical exchange may not be adequately described
(v) freezing of water and melting of ice are not modelled

Results from sample calculations with the proposed set of equations and parameterizations are presented. The bulk model was evaluated by comparison with observations and with simulations using a detailed 1D diffusion model, for a warm summer period in 2008 with large temporal variations of the water temperature. In all cases, the light attenuation characteristics derived from observations at a turbid water body and tuned to optimize the output from the 1D diffusion model were used initially. Three sets of calculations were performed with the bulk model:
1. using the meteorological conditions observed directly over the water body
2. using a set of standard meteorological observations from De Bilt, that requires one to estimate incoming solar radiation from a set of parameterizations
3. using basically the same meteorological observations from De Bilt, but with observed incoming shortwave radiation

The main features at hourly to monthly timescale were captured well or reasonably well in all cases. Using observed solar radiation from De Bilt (Case 3) instead of the parameterized one (Case 2) did not significantly improve the simulations for the period and location investigated here. The hourly temperature was estimated correctly (that is, within 1K) in 53-67% of the hours in the period investigated, depending on the quality of the input data. However, there was a tendency to overestimate the maximum temperatures in Case 1 and Case 2, resulting in a positive bias of 0.64 and 0.47 K, respectively. Case 3 showed a negative bias of 0.43 K. Reducing the turbidity considerably reduced the bias in Case 1 and Case 2 to 0.01 and -0.12K, respectively. At the same time, the percentage of correct hourly temperature estimates increases to 90% and 60%, respectively. In Case 3 the model performance deteriorated when lower values of turbidity were used.

It is assessed that the tendency for positive bias is related to ignoring the thermal stratification due to light absorption. Introducing a stability or density stratification indicator in combination with a surface temperature correction may repair this problem. However, finding an approach suitable for implementation in TOXSWA is beyond the scope of the present study and needs further analysis and investigation.

Some sample calculations are presented that demonstrate the sensitivity to depth in combination with light attenuation. Results from the proposed bulk system were compared only with results from simulations with a

detailed 1D diffusion model. The meteorological conditions observed directly over the water body were used to drive the models.

In natural systems with actively growing and decaying phytoplankton the light attenuation may be inversely proportional to depth. In such cases, the monthly average temperature will be rather insensitive to depth, because of compensating effects of light attenuation. However, if the light attenuation is independent of depth, the monthly averaged temperature and daily maxima increase with increasing turbidity (more light attenuation) until all available solar energy is being absorbed. For deep water, this natural maximum light absorption is reached at less turbid conditions than for shallow water, due to the longer light path-length in the former case.

Calculations of PPP degradation using the various temperature time series from observations and sample calculations were performed for a PPP with a dissipation half-life of 0.25 day, using the TOXSWA decay function. Daily temperature variations are expected to have the largest impact on such short-living PPP. Estimates of the average remaining PPP fraction stayed within 18% from the estimates using observed temperature. The results confirmed that the average remaining PPP fraction is correlated with mean temperature. Thus, bias will significantly influence deviations from calculations based on observed temperature. However, for the period investigated here the effect of diurnal temperature variations was estimated to be approx. 8%. The main advantage in using temperature variations at the time scale of one hour is that degradation dynamics of short-lived PPP can be included, which is needed for evaluation of application scenarios. In particular evaluation of PPP degradation in shallow, highly turbid waters may benefit from improved temperature estimates at a sub-daily timescale.

1 Introduction

1.1 Problem definition

The TOXSWA (TOXic substances in Surface WAters) model has been developed to describe the behaviour of plant protection products (PPP) in small surface waters and to estimate their concentration as a function of time. The degradation rate of PPP has a large impact on the evolution of their concentration. Estimation of the degradation rate of PPP in water is therefore an important part of the TOXSWA model.

The most common processes governing the rate at which PPP degrade are hydrolysis, photolysis and biotic degradation. Especially the rates of hydrolysis and biotic degradation processes are affected by temperature, usually adhering to an Arrhenius type of equation with activation energies often in the range of 50 - 100 kJ $mole^{-1}$ (Deneer et al., 2010). Consider, for example, a compound with a dissipation half life (DT50) of five days at 20 °C and with an activation energy for the dissipation process of 75 kJ $mole^{-1}$. Upon lowering the temperature to 10 °C, the DT50 will increase to almost fifteen days. This implies that dissipation will cause a daily concentration decrease of 13% at 20 °C, but of only 5% at 10 °C.

The example illustrates that a reasonable estimate of the water temperature is needed in order to get a good description of the decay of PPP in water. Decay rate constants and therefore the dissipation half-lives are related to temperature in an exponential fashion, due to the nature of the Arrhenius equation. The DT50 of various PPP vary between a few hours and a year. The shorter time scale implies that estimates of diurnal variations of water temperature may be required. This is because the exponential response of the decay rate constants to temperature implies that PPP with a higher degradation rate constant (smaller DT50) respond more sensitive to temperature fluctuations than PPP with a lower degradation rate constant (higher DT50). Thus, estimates of diurnal variations of water temperature may be required for PPP with fast degradation rates in particular.

The current version of the TOXSWA model uses monthly averages of the air temperature to describe the water temperature. As illustrated by the example given above, the use of average values for temperature will not take into account the relatively high degradation rates at elevated temperatures and may result in an underestimation of the rate of transformation and degradation reactions, in particular for PPP with high degradation rate constants.

Water bodies in the open air are influenced by the weather. On a long term basis variation in water temperatures are positively correlated with air temperature, predominantly because the air temperature is positively correlated with the amount of radiation absorbed by the water body. However, the effect of air temperature on the water temperature is quite indirect and depends on a suite of conditions in the atmosphere as well as in the water.

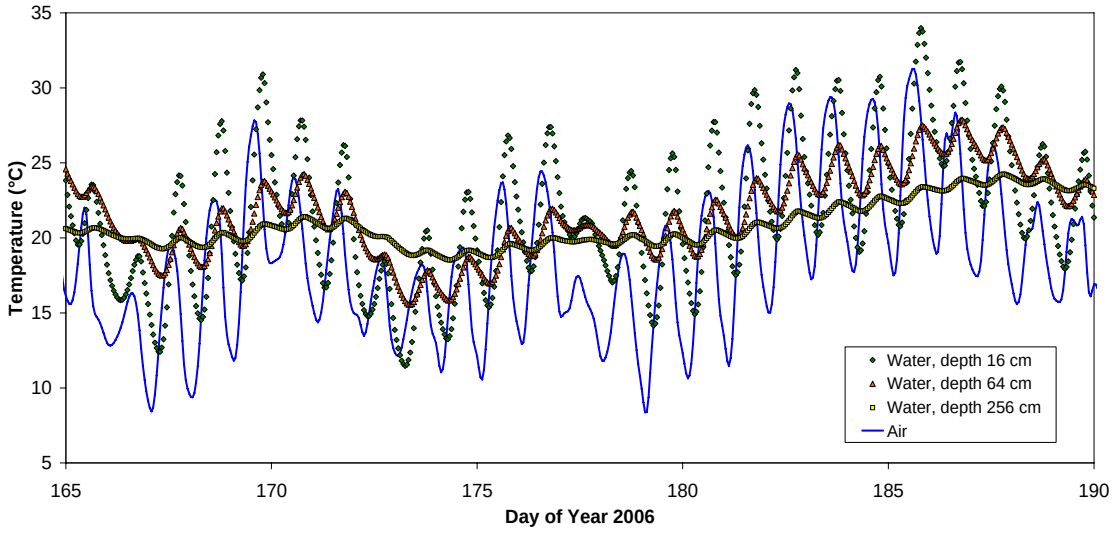

Figure 1.1

Water temperature in ponds of 16, 64 and 256 cm deep, and the air temperature at 1.5 m over the ponds. The water temperatures are simulated with a detailed model (Jacobs et al., 2002, 2009), for a warm period with often fine weather in the Netherlands, in the summer of 2006.

Because of the many processes involved, the response of water temperature of water bodies in a natural environment cannot be described reliably using only air temperature. This is illustrated in Figure 1.1, in which simulations of the water temperature in ponds with varying water depths are presented. The simulations were performed with a detailed physical model that describes the evolution of the water temperature as a function of the weather (Jacobs et al., 2009). The air temperature at 1.5 meters above the pond is also included in the figure. The period of time chosen here represents a summer situation with clear skies, implying high levels of incoming solar radiation during daylight hours and high levels of outgoing thermal (long wave) radiation during night time. Only for the shallow pond (16 cm water depth) there seems to be a clear relation between air and water temperature at a daily timescale, although the highs in water temperature seem to be somewhat delayed in relation to the highs in air temperature. In the deepest pond (256 cm water depth) there is only a relation at the time scale of a season, but with a clear delay.

It must be concluded that, in order to get a reasonable description of the response of water temperature to the weather, applicable at hourly to seasonal time scales and for various water depths, calculations need to be based upon the most important physical principles that govern the interaction between the atmosphere and the water. Next to natural influences of the weather on water temperature, artificial influences like drainage often apply. These influences also need to be included in the calculations.

1.2 Goal

The main goal of the study presented in this report is to provide suggestions for improvement of the algorithm in TOXSWA that computes the water temperature in small surface waters. The new algorithm should be able to simulate the temperature in small water bodies at hourly to seasonal timescales. It must provide physically realistic estimates with a target accuracy of 1K. Yet, the new algorithm must be as simple as possible and easy to implement in the existing TOXSWA environment. Data used to drive the model must be readily available.

1.3 Scope and limitations

Originally, the TOXSWA model was developed for ditches with slowly moving water in The Netherlands, but later on it was extended to simulate small streams and ponds with variable water levels and discharges as well. The main use of the current FOCUS_TOXSWA_2.2.1 model concerns the aquatic risk assessment for the registration procedure of pesticides at EU level. So, with respect to geographic extent the TOXSWA model is mainly applied in Europe. However, applications outside Europe, for example, in China, are at present being developed.

The FOCUS-TOXSWA model calculates exposure concentrations in ten standard scenarios across the EU and compares the exposure with ecotoxicological effect concentrations determined in test systems. The FOCUS surface water standard scenarios comprise a 30x30 m pond with a water depth of 1 m, and a 100 m long, 1 m wide ditch and stream. Water depth in the ditch is approximately 30 cm, while water depths in the stream range from 20 to 150 cm. The maximum levels may rise up to 2 or even 4 m in the near future when a series of years with more extreme weather conditions will be simulated. Discharges range up to 14 L s^{-1} for ditches, 500 L s^{-1} for streams and 1.6 L s^{-1} for ponds.

The water temperature calculations using the new algorithm should match the dimensions of surface waters modelled by TOXSWA as well as the level of detail of TOXSWA's process descriptions. Therefore, the description of water temperature is aimed at surface waters of a limited extent and water depth, such as (nearly) stagnant ponds, or ditches and small streams of a few metres wide. All three types of surface water in TOXSWA have water depths of a few metres at most. They are assumed to be well mixed over their cross-sectional area.

The water temperature description should be able to mimic the daily course of the water temperature because transformation half lives of PPP are known to range from hours to tens or hundreds of days. On the other hand it should not be too comprehensive since water temperature is only one of the factors determining transformation and transformation is only one of the many processes determining PPP behaviour.

Based on the aforementioned considerations, we selected a so-called integral energy model approach to describe the water temperature for the TOXSWA model. This type of model assumes one well-mixed water layer of uniform depth. The proposed concept corresponds well with the 'bulk' approach of TOXSWA. Basically, our approach will aim at a one-dimensional description to simulate air-water exchanges, that is, a description of vertical exchange processes. However, it can be easily extended into a quasi-two-dimensional approach by applying the bulk concept in a modular sense. Each module or segment is considered to be instantaneously well-mixed in the horizontal direction as well. Horizontal flows of heat due to temperature differences between the segments (advection) or other influences like energy input by drain water from adjacent fields can be described as a source or sink term in the individual segments. By choosing the segments to correspond to the segments used in TOXSWA's numerical solution, the proposed quasi-2D model corresponds well with the existing description of water flow implemented in TOXSWA.

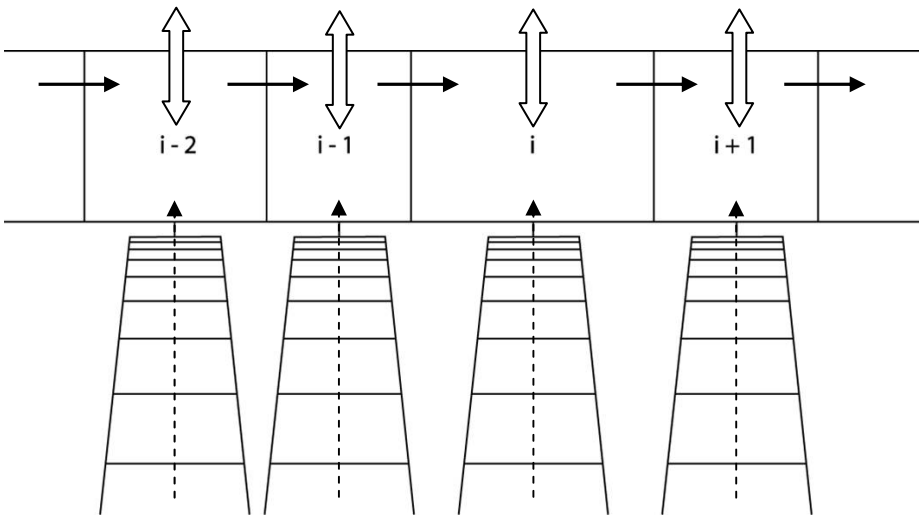

Figure 1.2

Comparison of the quasi-2D approach used in the present report to the quasi-2D approach in TOXSWA. The example displays a ditch viewed from the side. In TOXSWA, flow is considered in a horizontal direction, symbolized by control volumes i+n and the bold arrows. Each control volume can interact with the sediment below, where exchange flow between underlying segments is computed. This is symbolized by the connected surface elements at the bottom of the water layer and the dashed arrow. There is no interaction between the underlying segments in the direction of the flow. In the present report, the principal dimension is the vertical one in the water elements, illustrated by the open vertical arrows. The control volumes interact with the overlying atmosphere. The secondary, horizontal dimension is derived from the influence of an upstream element on a downstream one, and corresponds to the main flow direction in TOXSWA (bold arrows).

In order to avoid confusion it should be mentioned that TOXSWA also utilizes a 'quasi-2D approach', but using the horizontal dimension in the direction of the main flow as the principal direction. The second dimension may enter from a description of lateral, horizontal flow perpendicular to the main flow direction (see Figure 1.2). In the remainder of this report, the term 'quasi-2D approach' refers to the case where the vertical dimension is the main direction. Here, the second dimension enters if lateral, horizontal flow between control volumes is considered. This second dimension therefore corresponds to the principal horizontal dimension in TOXSWA.

The water temperature description proposed in this report has the following main limitations:

(i) The choice to implement a bulk approach implies that thermal stratification cannot be handled. Thermal stratification may occur in particular for somewhat deeper water bodies, with slowly moving water during daytime conditions of clear summer weather.

(ii) Light absorption in the water column is described following Lambert-Beer's extinction law. The impact of algae on the absorption of radiation in the water can be handled quite well in this way. However, the model will not necessarily be valid for systems where macrophytes dominate light absorption.

(iii) Walls may absorb, reflect and emit radiation. Walls above the water level may cast a shadow across the water, thus influencing short and long wave radiation exchange. A proper description of such processes would require complicated model extensions that are far beyond the level required in the present development of TOXSWA, while their impact on temperature is likely to be small in most cases. The influence of walls on radiation exchange is therefore excluded.

(iv) Processes such as entry of drainage water or runoff water from adjacent fields are considered as external sources or sinks of energy. This implies that the water temperature description is a function of these external entries and thus, that the quality of the water temperature simulation will be affected by the quality of the description of the external entries. This is especially important during periods in which the water body discharge is mainly composed of drainage flow or runoff. Cases where the influence of

external entries is exceptionally large as compared to the vertical exchange processes may not be adequately described by the present modelling concept.

(v) Freezing of water and melting of ice are not modelled in the present development of the model.

In spite of these limitations, it is expected that the proposed system will be sufficiently accurate for the purpose of describing the degradation of PPP in TOXSWA as a function of water temperature. This will be illustrated in a number of sample calculations based on the proposed modelling approach.

1.4 Structure of the report

The remainder of the report is structured as follows. Chapter 2 reviews the most important processes that determine the behaviour of water temperature in small water bodies. Based on these considerations, the modelling structure and formulations for implementation in TOXSWA have been chosen. The proposed formulations and parameterizations are discussed in Chapter 3. Finally, we will present some sample calculations based on the proposed modelling concepts in Chapter 4. Results from the sample calculations will be compared with results from a detailed model as well as with observations. Finally, a concluding summary is provided in Chapter 5.

2 Energy balance of open water

The processes that determine the temperature of a water body in the open air are schematically represented in Figure 2.1. We distinguish the following categories:

1. Exchange of energy at the air-water interface
2. Absorption of solar radiation absorption in the water
3. Exchange of heat with the sediment and the environment
4. Mixing in the water
5. Supply and extraction of energy through external mechanisms

Categories 1 - 4 are processes that will mostly occur naturally and are suited for a one dimensional (1D) description. Depending on the dimensions of the water body a two or three dimensional approach might be desirable. Category 5 processes are artificial processes like supply of drainage water as well as natural processes like surface runoff. We consider these mechanisms as 'external' because they can not take place through local natural exchange. The processes as mentioned in these categories will be discussed individually hereafter.

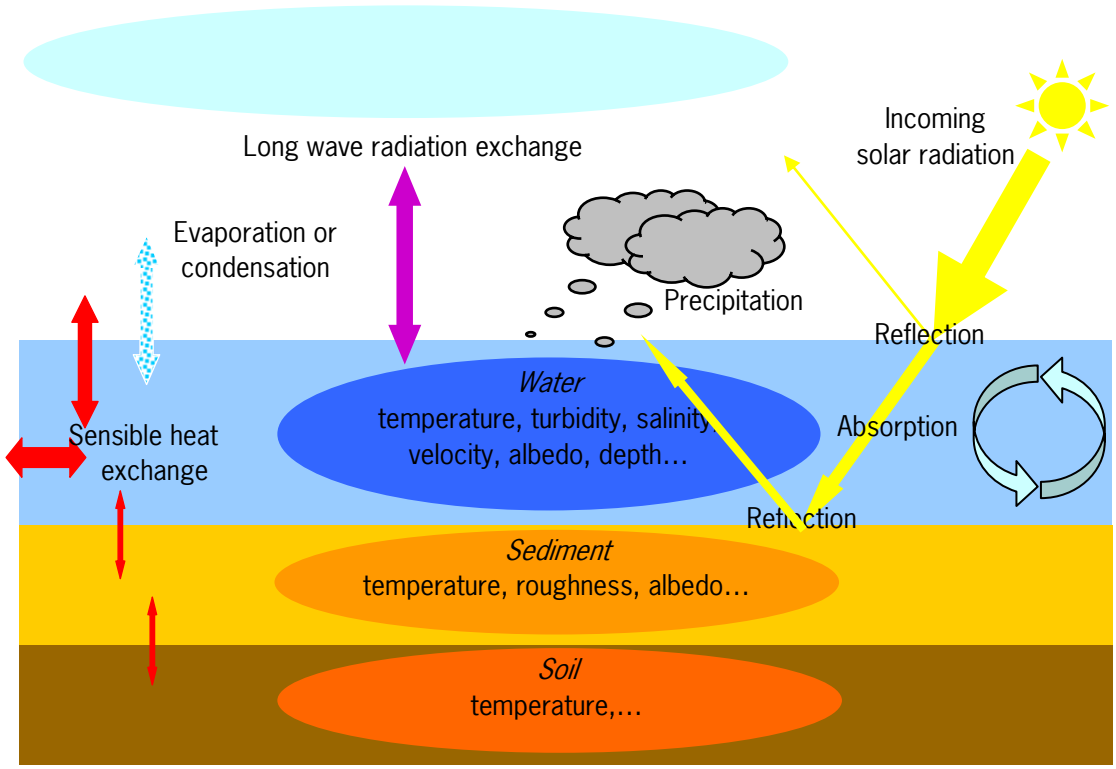

Figure 2.1

Schematic display of processes which determine the temperature of a water body. The ovals represent the four compartments of which information needs to be available to be able to calculate the energy balance. The most significant information is displayed. The straight arrows and the clouds represent energy flows and the curved arrows represent mixing.

2.1 Exchange with the atmosphere

The exchange of energy between water and the atmosphere progresses through transfer of sensible heat, evaporation and condensation, exchange of radiation and heat transfer through precipitation. The influence of shortwave radiation (solar radiation) is discussed in Section 2.2. Most of the discussed principles regarding the exchange processes used in the model can also be found in several textbooks like Stull (1988), Monteith en Unsworth (1990), Garratt (1992), Arya (2001) and Foken (2008).

Sensible heat
The transfer of sensible heat is driven by temperature differences between the water and the atmosphere. In this, the surface temperature of the water is leading. Increase in the temperature differences translates into increase of energy transfer. The sensible heat flux can be directed to or from the water. If directed from the water the water will slightly cool, if directed towards the water the water will heat up. Furthermore, a strong wind will stimulate the energy transfer because it creates a strong turbulence in the atmosphere which will ease mixing and transport of heat. Turbulence is also enhanced through positive vertical temperature differences (warm air is in a lower level), and suppressed by negative vertical temperature differences (cold air is at a lower level).

Evaporation and condensation
Transport of water vapour through evaporation and condensation provides for the transfer of latent heat. The energy needed for evaporation will be drained from the water, causing the water to cool down. In a reverse process condensation at the water surface will release energy which will slightly heat up the water. The transport of water vapour is driven by differences in amounts of water vapour between the water surface and in the atmosphere. A positive difference (more water vapour at the air-water interface than in the air) results in evaporation and a negative one in condensation. Identical to transport of sensible heat, strong winds and positive vertical temperature differences will stimulate transport of latent heat, but negative temperature differences will inhibit transport.

It may be assumed that the air at the water surface is saturated with water vapour. The water vapour concentration at the water surface can therefore easily be calculated using the surface temperature and salinity of the water. The amount of water vapour in the air is calculated using temperature and relative humidity of the air at the reference level (degree of saturation for water vapour).

Long wave radiation
All objects with a temperature above 0 K (≈ -273 °C) radiate heat and therefore lose energy. Vice versa they receive energy through absorption of radiation heat from other objects. The net long wave radiation balance depends on the temperature differences between objects and their emissivity (efficiency of radiation expressed on a scale from 0 to 1). The emission of long wave radiation is proportional to the absolute temperature to the fourth power, so minor temperature differences could lead to major radiation differences.
The emission of long wave radiation from the water surface is calculated from the surface temperature. The emissivity of the water is slightly less than 1. It is more difficult to calculate the return radiation from the atmosphere, because this radiation next to air temperature is also determined by humidity and the type and amount of clouds. Furthermore all layers of the atmosphere will contribute, each with their own temperature and humidity, all exchanging radiation energy with each other.

To assess the amount of down welling long wave radiation for water temperature calculations, observations would be preferred. However, such observations are not yet commonly available. The next best alternative would be to use the output from weather forecast models, in which the aforementioned processes are calculated in great detail. If measurements as well as output of weather forecast models are not available, the emissivity of the atmosphere can be estimated through one of many available simple parameterizations.

Combination of the estimated emissivity of the atmosphere with the air temperature at the reference level will give the flux of the incoming long wave radiation.

Precipitation
Precipitation on the water surface can heat or cool the water, depending on the temperature difference between the precipitation and the surface water and the intensity of the precipitation. The temperature of the precipitation is difficult to determine. It is assumed that the temperature of the precipitation close to the surface is approximately equal to the temperature of a well ventilated wet-bulb thermometer (Jacobs et al., 2008). These are thermometers with their bulb wrapped in wet muslin to determine the amount of evaporative cooling as moisture escapes from a surface. They are used in meteorology to determine the humidity of the air.

2.2 Absorption of radiation by the water

Absorption of solar radiation in the water column is a significant natural heat source for surface water, but with considerable variations on timescales from minutes to seasons. Therefore this process is very important to water temperature variations. Also thermal stratification of the natural open water is often directly related to the absorption of solar radiation.

Of the solar radiation at the water surface a small part is reflected immediately. Of the remainder, the radiation absorption in the water column needs to be calculated. Finally a part of the non-absorbed light can be reflected at the sediment and may subsequently be absorbed. The principles of these processes will be summarised next. We also will briefly discuss the possible effects of the walls of small water bodies.

Reflection at the water surface
The albedo or reflection coefficient is the ratio of reflected solar radiation to entering solar radiation. The albedo of water consists of two parts: the contribution from reflection of direct radiation, coming from the direction of the solar disc, and the contribution from diffuse radiation, coming from all hemispheric directions (Monteith and Unsworth, 1990). The albedo of direct light depends mainly on the position of the sun, while the albedo for diffuse light is almost constant (Graham Cogley, 1979).

The separate contributions to the total albedo can be determined from the fractions of direct and diffuse radiation. In their turn, these fractions can be estimated from the ratio of the total amount of sunlight entering at the surface and the theoretical maximum attainable solar radiation at the same place (Bindi et al., 1992). This ratio is an indication for the amount of clouds and therefore also for the fraction of diffuse light (De Rooy and Holtslag, 1999).

The maximum amount of sunlight results from astronomical calculations and depends on the latitude and the day of the year. It is preferred to get the total amount of incoming solar radiation at the earth surface from observations near the water body. Alternatively, this variable can be obtained from the output of the weather forecast model. If even this information is not available calculations can be done through one of many simple parameterizations.

Radiation absorption in the water column
The absorption of radiation in the water column is related to the wavelength and is determined by the amount of floating particles, algae and macrophytes (higher water plants).

In sunlight two important wavelength bands may be distinguished: wavelengths < 700nm and wavelengths > 700nm. Henceforth, we name these fractions PAR ('Photosynthetic Active Radiation', 400-700nm, used by plants for photosynthesis), and NIR ('nearby infrared, 700-1500nm), according to the most important

contribution to each band. The energy of the sunlight is approximately equally divided between PAR and NIR (Monteith and Unsworth, 1990).

The energy of the NIR band is for the most part almost immediately absorbed just beneath the water surface; the energy in the PAR band penetrates much further and decreases exponentially with increasing depth (Paulson and Simpson, 1977; Scheffer, 2004). The absorption within the PAR band depends on the characteristics of the absorbing parts of the water such as algae, waste products or floating sediment particles. This makes the attenuation co-efficient within PAR in principal dependent upon depth, but in turbid water and for shallow depths the effect is minor (Scheffer, 2004).

The attenuation co-efficient is wavelength dependent also within the previously mentioned wavelength bands. Depending on the purpose and the preferred accuracy of the energy balance calculations it is advisable to distinguish an appropriate number of wavelength bands, each with its own contribution to the energy in the sunlight and with its own attenuation coefficient.

The absorption of radiation in the water column is the most important cause of temperature variations at timescales between one hour and a season. The attenuation characteristics within the water column are therefore key characteristics in modelling the energy balance of water bodies. In some cases it is possible to estimate the attenuation coefficients from measurements of the light intensity above and within the water column. If there no observations are available, the attenuation characteristics can be used in model calibration. To limit the degrees of freedom, it can be useful to assume that the amount of radiation reaching the sediment is independent of the water depth. This implies the assumption that a given amount of algae develops in the water. The growth of algae is limited by light and if algae growth and algae mortality are balanced, a given fraction of PAR is being absorbed in the water column. This fraction is independent of depth and the amount of background turbidity which depends amongst others things on floating sediment particles (Scheffer, 2004). The attenuation coefficient for PAR will then be inversely proportional to water depth. Yet another alternative is to explicitly model the growth and decay of algae and predict the attenuation coefficient from the algal concentration (e.g. Reynolds et al., 2001). However, such an approach is beyond the scope of the present study.

Reflection from the sediment

For shallow water depths part of the light will reach the sediment. Part of this fraction can be reflected at the sediment and is available for absorption again. This can be regarded as an upward beam of radiation, starting from the sediment, additional to the downward radiation entering the water at air-water interface. Then, the absorption of both radiation streams can be treated in a physically identical way, through exponential attenuation.

The part of the radiation that is not reflected at the bottom will heat the sediment and subsequently also the water, through heat transfer from the sediment to the water.

Possible wall effects

In the above, possible edge effects on absorption of radiation have not yet been taken into account. This implies the assumption that in particular the ratio of the volume of the body of water to the surface of the edges is big. This assumption is possibly too coarse in the case of water bodies like narrow streams. In such cases the following effects possibly play a role:

- absorption of light by the walls
- effect of shadowing by the walls

The first effect is in practice is only of interest to the PAR wavelength, since the NIR part almost immediately is absorbed at the surface. The fraction absorbed PAR is determined by the albedo of the wall. Depending on the angle at which the PAR arrives at the surface, the path length of the absorbed light in the water can become

shorter than when the light would reach the bottom. In case of direct light the effective path length therefore depends on the solar elevation. The light reflected at the walls (typically about 20%-30%) continues its way through the water. The energy absorbed by the wall can partly be used to heat the water, which compensates partly for the shorter path length.

The second effect will be of interest to shortwave radiation as well as longwave radiation. Because of shadowing, relatively little solar radiation (shortwave) will reach the water. This effect applies only to the direct component of sunlight and is negligible at low sun position and high cloud cover. In sunny weather and with high position of the sun the fraction of direct light can increase up to 85% of the total radiation. The shadow effect can be partly compensated by reflection at the illuminated side of the ditch, but this compensation is at most equal to the effect of the albedo typically about 20%-30%.

The irradiation of longwave radiation will also be influenced by the walls. The walls will partly limit the radiation entering from the hemisphere. However, the walls themselves exchange radiation with the water surface. Because the effective emissivity of the air is generally much lower than that of the wall, the water will receive more longwave radiation than with an unblocked view of the hemisphere.

The net effect of the interaction of the walls with the radiation is expected to be small, and will depend on:
1. dimensions of the body of water (depth, width, length)
2. orientation of the body of water
3. slope of the wall
4. depth of the water surface below the surrounding field
5. properties (albedo, emissivity) and condition (temperature, moisture content) of the wall

2.3 Heat exchange with the sediment and the surrounding soil

It is usually assumed that the exchange of heat between water and sediments and with the surrounding soil is small. Hull et al. (1984), however, report 'unexpectedly large' energy flows between water and sediments, and between sediment and soil. Cathcart (1987) attributes errors in their model predictions to the absence of exchange with the sediment.

On the basis of these older studies Losordo and Piedrahita (1991) decided to model this exchange explicitly. The choice of parameter in their model approach 'leads to a realistic maximum'. An in-depth analysis of their results is however missing.

In a recent study, Paaijmans et al. (2008b) used observations and a model for an analysis of the contribution soil heat flux to the energy balance of shallow ponds in Kenya. They found a contribution of 0-2% of the total energy supply to the ponds and concluded that a detailed description of the energy exchange with the soil below the ponds was not required to properly describe the water temperature. Lamoureux et al. (2006) found on the basis of a model study a comparable contribution, of on average 1-5%, with a maximum 10% on some days in the winter, when the total energy supply was small.

Regarding lateral heat exchange with the surrounding soil, it appeared from the study of Paaijmans et al. (2008b) that this component was less than 1% of the total energy exchange for small ponds. This interaction may therefore be considered negligible in practice. Whenever this interaction is important is not clear. It is possible to imagine that the lateral heat-exchange in the case of the relatively narrow, but deep ditches do have a significant role in the energy balance of the water.

2.4 Vertical mixing of the water

The mixing of the water, among other things, determines the build-up of temperature stratification in the water. The density of water is increases with decreasing temperature. In fresh water the density is maximum at 4 °C and decreases again at lower temperatures down to the freezing point; the density of salt water continues to increase with decreasing temperature, until the freezing point has been reached (Gill, 1982).

Without mixing and with equal salinity a thermal stratification would arise as a result of the density differences related to temperature. The denser and colder water would remain below the warmer and less dense water. However this stratification is prevented by turbulence, which often mixes the water effectively. As a result, conditions with thermal stratification in shallow ponds are relatively rare (Scheffer, 2004). Time scales of vertical mixing are generally far less than one hour, depending on the depth. In not too deep waters with currents the assumption of a well-mixed water column in calculations of the temperature course over periods of time longer than this mixing time scale will give good results. In the past thermal stratification of the water was therefore often ignored or just crudely modelled. However, stratification can be seen in the summer, with sunny weather, in particular for stagnant water with greater depth (Jacobs et al., 2002).

Mixing is caused by the following three categories of processes:
1. effects of cooling and warming
2. air-water momentum exchange and momentum transport in the water column
3. density differences by salinity

The present research is focused on the temperature of freshwater bodies. Therefore, we will only discuss categories 1 and 2.

Effects of cooling and warming
Temperature variations arise by the processes described in the previous section. Depending on the nature of these temperature changes turbulence can be created and stimulated or on the contrary be suppressed (Gill, 1982; Kraus and Businger, 1994).

Cooling will predominantly take directly at the water surface. The processes involved are emission of longwave radiation, evaporation, sensible heat transport towards the atmosphere and cooling by precipitation. The water directly below the surface is therefore often slightly cooler than further away from the surface, a phenomenon called the 'cool skin (Katsaros, 1980). The cooler water tends to sink, causing a downward motion of the water, which in its turn leads to turbulence and therefore mixing of the water. Only by cooling through the sediment will cooler water be generated at the bottom which will somewhat suppress turbulence. For water depths of more than a few decimetres this heat flux will however be relatively small
(Paaijmans et al., 2008b).

Heating of water the water layer directly at the surface will take place by absorption of NIR (see Section 2.2), supply of sensible heat, condensation, and heating by precipitation. Absorption of PAR will take place over a greater vertical extent possibly down to the bottom of the water body depending on the conditions (see Section 2.2). Because the attenuation of PAR decreases with depth, water layers neat the top of the water column will heat up relatively fast. All in all the warming is the largest at the surface and this will tend to suppress turbulence. An exception is flow of heat from the sediment, the water heated to the bottom and a rising movement will deploy. An exception is the flow of heat from the sediment in which case the water at the bottom will heat up and cause a rising motion with associated turbulence. But this latter contribution will be small for water depths larger than several decimetres (Paaijmans et al., 2008b).

Sometimes, especially in summer during conditions of clear weather, the combination of these processes causes a diurnal variation in mixing and thermal stratification. At night cooling at the surface will be stronger, whereby turbulence and mixing is stimulated. During the day, with strong solar irradiation, warming will prevail. This warming decreases with depth, which can result in stabilisation and stratification.

Air-water momentum transfer and momentum transport in the water column
Momentum transfer of the atmosphere to the water is caused by the wind. Near the surface the wind is slowed down, which causes the momentum transfer. The transfer increases as the water surface gets rougher, because of increasing wave height and breaking waves (Garratt, 1992; Kraus and Businger, 1994). The momentum transfer creates turbulence and therefore mixing.

Breaking waves also result in turbulence. This concerns not only the breaking related to the visible phenomenon accompanied by white crested waves, the whitecaps (Terray et al., 1996), but also the invisible breaking of microscale waves that are already present at low wind speed (Csanady, 1990). To calculate momentum transport by breaking waves, the characteristics of the wave field should be known.

In the water vertical differences in current, shear, also lead to turbulence. These current differences are created both at the surface under the influence of the wind and close to the bottom by interaction with the sediment. The water surface tends to move along with the wind near the surface. This causes shear just below the water surface, depending on the wind speed and direction relative to the water current. At the sediment, friction causes the water to slow down, again causing shear. It may be assumed that the current is zero at the sediment surface itself. The shear between these two borders causes mechanically generated turbulence. However, the shear in its turn depends upon the turbulence (Troen and Mahrt, 1986; Large et al., 1994).

2.5 Supply or extraction of energy through external mechanisms

In addition to the previously described direct interaction of water bodies with their environment, natural or artificial influences may exist that can be described as a source or a sink of heat in an otherwise vertical framework. An example of such a natural source or sink is the precipitation runoff to a ditch from surrounding land. The temperature of rainwater will be modified by the interaction with the soil before it enters the ditch. Examples of artificial influences are the supply or extraction of heat for conditioning of the water temperature in aquaculture ponds, or supply of water through an artificial drainage system.

In a 1-D context such influences can be considered as an external or independent source or sink of energy in the water column. The size of this source or sink is given by the difference in the energy content of the water in the water body under consideration and the water that is being supplied, in combination with the flow rate of the water supply. Energy content per unit volume is given by the heat capacity, the density and temperature of the water. Under the assumption of perfect mixing the source or sink strength can then be expressed as a heat flux per unit horizontal surface area. In case of direct heating or cooling the strength of the source or sink is simply given by the power supply per unit surface area.

The hypothesis of immediate perfect mixing is in practice often a reasonable one at timescales for one hour and longer. The vertical mixing processes (see Section 2.4) generally have time scales of much less than an hour, depending on the depth. In addition, horizontal mixing is in practice often accomplished by recirculation systems, artificial mechanical mixing or conditioning systems which cover a large part of the body of water horizontally. This also implies conditions approaching horizontal homogeneity. Drainage of rainwater in a ditch can in many cases probably be regarded as a line source. In the case of water bodies that are not too wide, the hypothesis of good blending would then also be reasonable. For strong point sources, where large

temperature differences prevail between the water in the water body of interest and the water supplied by the source, the hypothesis of immediate full mixing will in some cases no longer be valid.

3 Implementation

3.1 Selection of the modelling concept

In the scientific literature, numerous models to simulate the temperature of water bodies have been described, for various applications. Most often the starting point is a 1D framework. For most applications, this leads to quite acceptable results in practice. A 1D approach can easily be put in a (quasi-) 2D (two-dimensional) framework.

Two groups of 1D models can be distinguished:

1. Diffusion models that describe the temperature profile in the water column in quite some detail. This requires explicit treatment of turbulence. This group of models allows studying thermal stratification as well. Examples are the model for the Northsea described by Jacobs et al. (2002) and the shallow water model described by Jacobs et al. (2008).
2. Integral energy models, which describe the water temperature uniformly. This class of models varies from bulk models, assuming one well-mixed layer to models that distinguish a limited number of layers where in each individual layer the temperature is assumed to be well-mixed. Examples are the model to simulate the temperature behaviour in aquaculture ponds described by Losordo en Piedrahita (1991) and the model for temperature estimation of shallow water pools by Paaijmans et al. (2008a).

For many practical applications, the assumption of a well-mixed water layer appears to be sufficiently accurate, in particular when the water depth is low, typically less than ~1m, depending on climatologic conditions, current and availability of mixing devices such as pumps in aquaculture ponds. Of course, the most important components of the energy balance, notably the fluxes at the air-water interface and the bulk absorption of solar radiation in the water column have to be modelled with reasonably accuracy. Errors in the energy budget arising from the fact that temperature gradients near the surface or at the water-sediment interface are neglected are probably acceptable for most applications. To describe the fluxes at the lower boundary of the water column, the water-sediment interface, the energy budget and thermal behaviour of the sediment layer must be known as well. The temperature of the sediment can also be modelled dynamically, which leads to a by-product of a model for the water column that may be convenient in the context of some of the TOXSWA applications.

A bulk model can be applied quite easily in a quasi-2D framework (cf. Jacobs et al., 2002). This is because the bulk concept can be used in a modular sense, which also allows external source and sink terms to be defined straightforwardly. Advection of heat can be parameterized as such an external source or sink term (see Section 2.5). A similar extension can be made in diffusion models, but this would require the vertical distribution of sources and sinks in the water column to be specified. In both cases, extension to a quasi-2D framework relies on the assumption that the control volume is well-mixed horizontally, that is, the control volume is assumed to be horizontally homogeneous. This assumption is already in place in TOXSWA.

Based on this assessment, we conclude that it is advisable to design for use in TOXSWA a 1D-bulk model for simulation of the thermal behaviour of surface waters bodies. This approach matches the bulk concepts (i.e., well-mixed control volumes) used to model water flow in TOXSWA and can therefore easily be integrated in that model. The bulk approach is a convenient framework to include effects of various external impacts on the energy budget, such as advection and artificial heating. It is physically realistic and yet simple to apply. It does

not require a detailed description of turbulence and density effects on stratification. Finally, the data requirement is limited.

In de next section we describe the main modules that a reasonably accurate bulk model should contain.

3.2 Design of a bulk model to describe the thermal behaviour of open water bodies

The energy budget of a horizontally and vertically homogeneous water body in contact with the atmosphere and with depth h [m] is given by:

$$K_d - K_u + L_d - L_u - H - \lambda E + G_s + Q_{pr} + \sum S = \rho_w c_w h \frac{\Delta T_w}{\Delta t} \quad (1)$$

where

ρ_w = density of the water, ≈ 1000 [kg m^{-3}]
c_w = specific heat capacity of the water, ≈ 4.19·10^3 [J kg^{-1} K^{-1}]
T_w = temperature of the water [K]; ΔT_w= temperature difference [K]
t = time [s]; Δt = time interval considered [s]
K_d = incoming shortwave (solar) radiation [W m^{-2}]
K_u = reflected shortwave (solar) radiation [W m^{-2}]
L_d = incoming longwave (thermal) radiation [W m^{-2}]
L_u = outgoing longwave (thermal) radiation [W m^{-2}]
H = sensible heat flux at the air-water interface (positive upward) [W m^{-2}]
λ = latent heat of vaporisation of water ≈ 2.46·10^6 [J kg^{-1}]
E = water vapour flux at the air-water interface (positive upward) [kg s^{-1} m^{-2}]
G_s = sensible heat flux at the water-sediment interface (positive upward) [W m^{-2}]
Q_{pr} = exchange of heat through precipitation [W m^{-2}]
ΣS = sum of other heat sources and sinks [W m^{-2}]

Here, we understand 'depth' to be an effective or characteristic water depth, defined by the ratio of volume V [m^3] to horizontal surface area O_x [m^2], i.e. V/O_x, of the control volume. The individual terms in (1) will be discussed in more detail in the following subsections.

3.2.1 Shortwave radiation

For good modelling results, it is essential that the down welling shortwave radiation balance is estimated as accurately as possible. In particular during daytime in summer, the net shortwave radiation (K_d-K_u) is one of the major controls of the temperature variations, along with the net longwave radiation (L_d-L_u).

For the best accuracy, it is preferred that K_d is taken from observations nearby the modelled water body. However, in cases where such observations are not available, K_d should be estimated from meteorological observations performed at a standard weather station. Sometimes, direct observations of K_d are reported at such a station. In other cases, a simple parameterization has to be used to estimate K_d from the set of standard meteorological observations. Many of such parameterisations, based on a calculation of solar elevation (φ [radians]) and an estimation of the atmospheric turbidity and cloud cover, are available.

A practical estimate of solar elevation is obtained from (cf. Stull, 1988):

$$\sin\varphi = \sin\delta \sin\Phi + \cos t_h \cos\delta \cos\Phi \quad (2)$$

where Φ [radians] is the local latitude (positive north), δ [radians] = 0.409cos(2π(D-d_s)/365.25) is the declination of the sun (with D [-] the day of year and d_s = 171 [-] is the day of the summer solstice). Furthermore, t_h [radians] is the hour angle, approximated as t_h = (πt_d/12 - Λ – π) (with t_d [h] the time of day in UTC and Λ [radians] the longitude (positive west)).

A well-known and widely used parameterisation to compute K_d from solar elevation is the one by Holtslag and van Ulden (1983). Under clear skies,

$$K_d = K_d^0 = a_1 \sin\varphi + a_2 \tag{3}$$

where a_1 [W m^{-2}] and a_2 [W m^{-2}] are empirical coefficients describing the average atmospheric attenuation of shortwave radiation at a given site. For De Bilt (Netherlands), a_1 = 1041 W m^{-2} and a_2 = -69 W m^{-2}. Under cloudy skies K_d becomes

$$K_d = K_d^0(1 + b_1 N^{b_2}) \tag{4}$$

with N [-] the total cloud cover and b_1 [-] and b_2 [-] are empirical coefficients. Values for b_1 and b_2 derived from measurements in Western Europe are -0.75 and 3.4, respectively.

For small water bodies where the water surface is well below the surrounding land surface, K_d may have to be corrected for the shielding effect by the walls (Jacobs *et al.*, 2008), but for the time being we ignore this effect.

A fraction α_t of K_d is reflected directly at the water surface, with α_t [-] denoting the albedo of the water surface, which has a maximum value of 1. The total albedo consists of two components, one due to reflection of direct light, α_{dir} [-], and one due to reflection of diffuse light, α_{dif} [-]:

$$\alpha_t = f\alpha_{dir} + (1 - f)\alpha_{dif} \tag{5}$$

where f = the fraction of direct radiation = K_{dir}/K_d [-], with K_{dir} [W m^{-2}] the flux of direct shortwave radiation. Component α_{dif} is approximately constant with a typical value of 0.06. Component α_{dir} is given by the Fresnel albedo which depends on the solar zenith angle Z= (π/2 - φ) and refraction angle r = sin^{-1} (sin(Z)/1.33) [-]. For $\varphi > 0$ (Graham Cogley, 1979):

$$\alpha_{dir} = 0.5\left[\frac{\sin^2(Z-r)}{\sin^2(Z+r)} + \frac{\tan^2(Z-r)}{\tan^2(Z+r)}\right] \tag{6}$$

The amount of direct radiation in the solar radiation at the surface can be measured, but such observations are not performed on a routine basis. Therefore, in most cases parameterisations will have to be used to determine the fraction f in (5). Such formulations are based on the atmospheric transmissivity τ_a [-], that can be approximated by (De Rooy and Holtslag, 1999):

$$\tau_a = \frac{K_d}{1367\sin\varphi} \tag{7}$$

In (7) K_d can be taken from observations or from parameterisation (2)-(4). Bindi et al. (1992) compared a number of parameterisations to estimate the fraction of diffuse light, that is, (1-f). They found the one by Erbs et al. (1982) to perform reasonably well at hourly to daily timescale. That parameterisation reads:

$$\begin{cases} 1-f = 1-0.09\tau_a & \tau_a \le 0.22 \\ 1-f = 0.9511-0.1604\tau_a+4.388\tau_a^2-16.638\tau_a^3+12.336\tau_a^4 & 0.22 < \tau_a \le 0.80 \\ 1-f = 0.165 & \tau_a > 0.80 \end{cases} \quad (8)$$

The fraction (1- α_t) of K_d that is not reflected directly at the water surface enters the water column and will partly be absorbed in the water column. From the radiation that reaches the bottom of the water column a fraction equal to the albedo of the sediment, α_b [-], will be reflected. Part of this radiation will also be absorbed in the water column; the remainder will leave the water again and contributes to K_u. For our purpose, it is sufficiently accurate to treat the upward beam and the downward beam separately, that is, as if they are independent of each other.

The process of absorption is described using Lambert-Beer's extinction law. Then, for the downward beam, the distribution of the radiation in the water column becomes (cf. Paulson and Simpson, 1977):

$$K^{\downarrow}(d) = (1-\alpha_t)K_d \sum_{j=1}^{n} \xi_j \exp(-\mu_j d) \quad (9a)$$

where $K^{\downarrow}(d)$ [W m^{-2}] is the energy in the downward beam as a function of the distance d [m] from the water surface, ξ_j [-] is the energy fraction of Kd contained in wavelength band j [-] and μ_j [m^{-1}] the extinction or attenuation coefficient in that wavelength band. Thus, at the bottom of the water column, where $d=h$:

$$K^{\downarrow}(h) = (1-\alpha_t)K_d \sum_{j=1}^{n} \xi_j \exp(-\mu_j h) \equiv K_{bot}$$

The amount of upward radiation after reflection at the sediment then equals $\alpha_b K_{bot}$. For the upward beam, denoted with $K^{\uparrow}(d)$, we therefore have:

$$K^{\uparrow}(d) = \alpha_b K_{bot} \sum_{j=1}^{n} \exp(-\mu_j (h-d)) \quad (9b)$$

Since d=0 at the water surface, and ignoring refraction of the upward beam at the water surface:

$$K_u = \alpha_t K_d + \alpha_b K_{bot} \sum_{j=1}^{n} \exp(-\mu_j h) \quad (10)$$

Equation (10) represents that total upward shortwave radiation at the air-water interface and includes the amount of radiation directly reflected at the surface ($\alpha_t K_d$). Note that, in particular for larger water depths with h ~1m or more and for very turbid water, the second term on the right hand side can become very small and may be neglected.

In the bulk approach, implicit in (1), only (K_d-K_u) needs to be known and details on the radiation profiles in the water columns are not required. However, for some applications such as assessment of thermal stratification or computation of photolysis rates, the vertical distribution of radiation in the water column needs to be taken into account explicitly. To obtain a first-order estimate of the radiation profiles in such cases, the energy contained in the downward beam (9a) and in the upward beam (9b) can be added at specified levels of d, which then gives the total radiation flux as a function of depth.

In the present development there is no need for a detailed description of the light spectrum. Therefore, we distinguish two wavelength bands, the NIR and the PAR band. Then, n in (9) and (10) is equal to 2 and we only need to specify energy fraction ξ and attenuation coefficient μ for those two bands. In particular ξ is quite well known and can easily be obtained from observations.

When distinguishing the PAR and the NIR bands only, the attenuation coefficient for the NIR band simply needs to be large enough to ensure that all the energy contained in NIR is absorbed just below the surface, within the first millimetre, say. However, the simulations are quite sensitive to the attenuation coefficient for PAR. In the present development this parameter can be used to calibrate the model. The coefficient can also be estimated from observations.

Jacobs et al. (2009) fitted μ for PAR to observations of light intensity under water. The value of μ reported by Jacobs et al. (2009) is given in Table 3.1, along with a default value that was obtained from a fit to the light absorption characteristics used by Jacobs et al. (2008). The value from Jacobs at al. (2009) was obtained in a pond with a water depth of 32 cm. It can, arguably, be regarded as appropriate for, on average, turbid water. For a water column of height 32 cm it results in a unidirectional attenuation of 74% for the energy in the PAR band, and of 86% for PAR+NIR. By comparison, the values fitted to the default absorption characteristics used by Jacobs et al. (2008) yield a unidirectional attenuation of 54% for PAR, and 75% for PAR+NIR over a water depth of 32 cm. They are appropriate for moderately clear water.

For depths other than 32 cm, the coefficient can be adjusted to give the same light attenuation over the entire water column. This implies the assumption that growth of algae is limited by light and if algae growth and algae mortality are balanced, a given fraction of PAR is being absorbed in the water column (see Section 2.2). However, in some cases if the water quality is dominated by physic-chemical influences rather than by biological mechanisms, a constant absorption coefficient may be more appropriate.

Table 3.1

Proposed default values for a two-wavelength band extinction model based on (9a), (9b) and (10). Default values for energy fraction ξ are taken from Jacobs et al. (2008). Two sets of values are given for attenuation coefficient μ : 1) a default value that was obtained from a fit to the light attenuation modelled by Jacobs et al. (2008); 2) values derived from measurements in a 32 cm deep pond with high turbidity due to abundant presence of algae.

Wavelength Band	Energy fraction ξ [–]	Attenuation coefficient μ[m^{-1}]	
		Default	Turbid
1. NIR	0.45	1000	1000
2. PAR	0.55	2.52	4.25

3.2.2 Longwave radiation

For good modelling results, it is essential that the net longwave radiation balance (L_d - L_u) is estimated as accurately as possible. On a yearly basis L_d is the largest source of natural energy and during wintertime in particular the temperature variations are to a large extent determined by (L_d - L_u).

It is preferred that L_d is taken from observations nearby the modelled water body. Alternatively, L_d can be estimated from one of the many algorithms that are based on readily available meteorological quantities. De Rooy and Holtslag (1999) obtained satisfactory results for the Netherlands using:

$$L_d = \varepsilon_r \sigma T_r^4 + c_2 N - c_3 (N - N_h) \tag{11}$$

where ε_r [-] is the apparent emissivity of the atmosphere, $\sigma = 5.67 \cdot 10^{-8}$ [W m^{-2} K] is the Stefan-Boltzmann constant, T_r [K] is the air temperature at the reference height (taken 2m above the surface), $c_2 = 70$ [W m^{-2}] and $c_3 = 50$ [W m^{-2}] are empirical coefficients and N_h [-] is the fraction of middle and low cloud. Parameterisation (11) can also be applied without the correction term for high clouds, that is, with $c_3 = 0$. Furthermore,

$$\varepsilon_r = 1.2\left(\frac{0.01 e_s(T_r) H_r}{T_r}\right)^{1/7} \tag{12}$$

(Brutsaert, 1982) with H_r [-] the relative humidity at the reference level and $e_s(T_r)$ [Pa] the saturation vapour pressure at the air temperature (see equation 18b). The factor 0.01 is used for unit scaling, from [Pa] to [hPa].

The outgoing longwave radiation is given by:

$$L_u = \varepsilon_w \sigma T_w^4 + (1 - \varepsilon_w) L_d \tag{13}$$

where ε_w [-] is the emissivity of the water. A good estimate of the latter quantity is ε_w = 0.97. For specific cases, the emissivity can be estimated from radiation measurements (Jacobs et al., 2009). Formally, T_w should be taken equal to the water temperature at the surface, but in the context of a bulk model it is estimated from the temperature in the bulk layer of the water.

In case of small water bodies where the water surface is well below the surrounding land surface, L_d may have to be corrected for interactions between the walls and the water surface (Jacobs et al., 2008), but for the time being we ignore this effect.

3.2.3 Turbulent fluxes

The next two terms in (1), H and λE represent the link between the water and the atmosphere through turbulent exchange of heat and moisture. Depending on the temperature and moisture difference in the atmosphere, between the reference level z_r [m] and a level almost at the water surface, the exchange may be a source a sink of energy to the water body. According to micrometeorological convention, the turbulent fluxes are taken positive upward, representing a sink, and the reverse.
Over water surfaces, a so-called bulk approach is commonly applied (e.g., Losordo and Piedrahita, 1991; Jacobs et al., 2002; Paaijmans et al., 2008a). In this concept,

$$H = \rho_a c_a C_H u_r (T_w - T_r) \tag{14}$$

and

$$\lambda E = \rho_a \lambda C_E u_r (q_s(T_w) - H_r q_s(T_r)) \tag{15}$$

Here, ρ_a [kg m^{-3}] = p_a/RT_r is the density of the air (with p_a [Pa] the atmospheric pressure at the surface and R = 287 [J kg^{-1} K^{-1}] the specific gas constant for dry air, C_H [-] and C_E [-] are the bulk transfer coefficients for heat and moisture, respectively, $c_a \approx$ 1005 [J kg^{-1} K^{-1}] is the heat capacity of the air, u_r [m s^{-1}] is the wind speed at the reference level at height z_r, T_r [K] the air temperature at z_r, H_r [-] the relative humidity at z_r and $q_s()$ [kg kg^{-1}] the saturation specific humidity at the given temperature. Note that $\lambda E/\lambda = E$ is a mass flux in kg m^{-2} s^{-1}, which also corresponds to a mass flux in mm s^{-1} (per m^2) and can directly be used in water balance calculations.

In principle, C_H and C_E depend on the atmospheric stability between the surface and reference height z_r. However, for the purpose of computing the energy balance of water surfaces, results without taking these stability effects into account are quite satisfactory. Therefore, the bulk transfer coefficients may be taken constant. Over large water surfaces, such as over the sea but also over large aquaculture ponds $C_H = C_E$ = 0.0011 is adequate (DeCosmo et al., 1996; Jacobs et al., 2009). For small water bodies the turbulent characteristics over the water are completely governed by the surrounding land surface characteristics so that C_H and C_E may be somewhat larger. Paaijmans et al. (2008a) found good results with C_H=C_E=0.003, for a

tropical water pool. The latter value was derived for a small water surface surrounded by short grass. In general, for neutral conditions the bulk transfer coefficients over land between the surface and height z_r is given by:

$$C_H \approx C_E = \frac{\kappa^2}{\ln(z_r/z_0)\ln(z_r/z_h)} \tag{16}$$

where z_0 [m] is the aerodynamic roughness, z_h [m] ≈ $0.1 z_0$ is the roughness length for heat and κ ≈ 0.4 [-] is the Von Kármán constant.

Wind speed u_r has to be taken from meteorological observations or from output from a meteorological model. It is routinely measured at weather stations, but it is usually given at a height of 10m. However, the wind speed at z_r can be estimated from the observed wind speed u_{obs} [m s^{-1}] at any observation height, z_{obs} [m], using the so called logarithmic wind profile. Neglecting stability effects again

$$u_r = u_{obs}\left[1 - \ln(z_{obs}/z_r)/\ln(z_{obs}/z_0)\right] \tag{17}$$

The aerodynamic roughness in (17) formally applies at the site of the wind speed observations, usually a grassland site with z_0 ≈ 0.02 m. If the roughness surrounding the water body differs much from that value, additional corrections may have to be applied.

Finally, in order to compute the evaporation, $q_s(T)$ can be obtained from (Monteith and Unsworth, 1990):

$$q_s(T) = \varepsilon \frac{e_s(T)}{p_a} \tag{18a}$$

with

$$e_s = 611\exp(17.27(T-273)/(T-36)) \tag{18b}$$

[Pa] is the saturation vapour pressure, T [K] is the absolute temperature and ε = 0.622 [-] is the ratio of the molecular mass of water vapour to that of air.

Equations (14)-(18) allow the turbulent fluxes H and λE to be estimated from specifications of the wind speed, temperature, relative humidity and atmospheric pressure at the reference level z_r. These quantities are readily available from standard meteorological observations. They should be obtained as close as possible to the location of interest, which may require interpolation between a number of meteorological stations. Nevertheless, it will be difficult to account for all local effects on the meteorological conditions if on-site observations are not available. Output from sophisticated meteorological models may be a good alternative to obtain the required data. Note that the water temperature is taken from the model simulations and does not require external input, except for the specification of an initial water temperature.

3.2.4 Interaction with the sediment

The heat flux between the sediment and the water is generally only a small term in the total heat budget of a water column (Paaijmans et al., 2008b) and therefore does not require a detailed modelling approach. A bulk approach that neglects temperature differences within the sediment layer was found to give satisfactory results for various water bodies (Losordo and Piedrahita, 1991; Lamoureux et al., 2006; Jacobs et al., 2009). Using that approach, the heat exchange between the sediment and the water, can be modelled as (Losordo and Piedrahita, 1991):

$$G_s = \frac{k_{sed}(T_{sed} - T_w)}{0.5 D_{sed}} \tag{19}$$

where T_{sed} [K] is the temperature of the sediment, k_{sed} [W m^{-1} K^{-1}] is the heat conduction coefficient of the sediment, and D_{sed} [m] is the depth of the sediment layer.

The temperature of the sediment, T_{sed}, can be taken from observations of the soil temperature at the depth of the sediment layer. Jacobs et al. (2009) found that good results can also be obtained using observations that are performed somewhat further away, as long as the wave characteristics given by (20) represent the regional climate. Alternatively, T_{sed} can also be computed using a diagnostic approach as in Lamoureux et al. (2006):

$$T_{sed} = \frac{T_{amp}}{D_{damp}}\left[\sin(\omega t + \vartheta) + \cos(\omega t + \vartheta)\right] \tag{20}$$

where T_{amp} [K] is the amplitude of the annual temperature wave of the sediment layer, D_{damp} [m] the damping depth, ϑ [rad] a phase shift and ω = 2,738□10^{-3} [day^{-1}] is the frequency of the period considered. Using this value for ω, (2) yields T_{sed} at a daily basis. All parameters in (20) can be determined from long-term soil temperature observations. Evidently, it is preferred to observe the soil temperature near the location of interest.

If no observations of soil temperature are available, the sediment temperature can be computed dynamically using a set of simple heat transfer equations (Losordo and Piedrahita, 1991). In that approach changes in T_{sed} are given by:

$$\rho_w c_w D_{sed} \Delta T_{sed} = \Delta t (G_{K\downarrow} + G_{gw} - G_s) \tag{21}$$

where

$$G_{K\downarrow} = (1-\alpha_b)(1-\alpha_t) K_d \sum_{j=1}^{n} \xi_j \exp(-\mu_j h) \tag{22}$$

[W m^{-2}] is the amount of light absorbed by the sediment, and

$$G_{gw} = \frac{k_{soil}(T_{gw} - T_{sed})}{\Delta z_{gw}} \tag{23}$$

[W m^{-2}] represents the heat exchange between the groundwater and the sediment. In (23), k_{soil} [W m^{-1} K^{-1}] is the heat conductivity of the soil, T_{gw} [K] is the temperature of the groundwater and Δz_{gw} [m] is the distance between the groundwater and the sediment.

Note that in (21) the density and heat capacity of the water are used. This is justified because the sediment is oversaturated with water and largely adopts the properties of water. This also implies that in (19) we may take the heat conductivity for water to estimate k_{sed}, that is, k_{sed} = 0.57 W m^{-1} K^{-1}.

To estimate G_{gw} the T_{gw}, k_{soil} and Δz_{gw} must be known. T_{gw} usually is quite constant. If data of T_{gw} are not available, it may be estimated as the climatological mean of the air temperature at the location of interest. For k_{soil} a global average of 2.4 Wm^{-1}K^{-1} appears to give satisfactory results (Hull et al., 1984). Finally, Δz_{gw} has to be estimated from observations, or may be optimized to give realistic results for the temperature wave in the sediment.

For water bodies such as natural ponds and ditches, an additional correction can be applied to G_s to account for heat transport through the walls, assuming that the mean soil heat flux at the walls is similar to the one at the bottom. The correction factor then simply equals the ratio of the wall surface to the bottom surface (Paaijmans et al., 2008a). In case of a circular pool with radius r [m] $G_s = G_{s0}(1+2h/r)$, with G_{s0} the uncorrected heat exchange with the soil. In case of a water body with length l [m] and with w [m], $G_s = G_{s0}(1+2h/l+2h/w)$, which approaches $G_s = G_{s0}(1+2h/w)$ in case of a ditch where $l \rightarrow \infty$. However, note that in many cases, G_s is small as compared to other energy fluxes and such a correction factor can be ignored in practice.

3.2.5 Precipitation

Heat exchange due to precipitation, Q_{pr}, can be estimated by assuming that the temperature of the raindrops, T_p [K] approaches the wet bulb temperature near approach the earth's surface (Jacobs et al., 2008):

$$Q_{pr} = \rho_w c_w P_l (T_p - T_w) \tag{24}$$

where P_l [m s^{-1}] is the rain rate. The wet bulb temperature is one of the routinely reported weather data from meteorological stations. It can also be estimated from the temperature and relative humidity at the reference level, T_r and H_r, respectively (cf. Monteith and Unsworth, 1991):

$$T_p \approx T_r - \frac{(1-H_r)e_s(T_r)}{66 + s(T_r)} \tag{25}$$

with $s(T_r) = \lambda e_s(T_r)/(462 T_r^2)$ [Pa K^{-1}] is the rate of increase of the saturation vapour pressure with temperature evaluated at T_r.

The amount of precipitation is also available from weather reports. Since this quantity can be highly variable in space and time significant errors in P_l may arise when allocating the reported amounts to the location and the time interval of interest. However, because the contribution of this term to (1) is generally quite small, this error is usually not critical when estimating water temperatures.

3.2.6 Bulk sink and source terms and link to quasi-2D approach

In the concept described here, any other process leading to changes in the heat content of the water can be easily implemented owing to the assumption of well mixed conditions. The energetic impact is included via the ΣS-term in (1), which requires that the contributions have to be expressed on an (horizontal water surface) area basis, that is, terms of W m^{-2}. Evidently, the physical background of such processes has to be properly defined for each individual case. Here, two examples will be discussed that are important in the framework of studies with TOXSWA: 1) input of water via drainage or surface runoff; 2) advection of upstream water. In both cases, immediate mixing in the control volume is assumed. This is consistent with the modelling framework of TOXSWA.

1) Input of water via drainage or surface runoff

Under horizontally homogeneous conditions and assuming that changes in water depth in a time step Δt are small, the heat exchange due to input of water from drainage or surface runoff, S_{dr} [W m^{-2}] can be described as:

$$S_{dr} = \rho_w c_w F_{dr} (T_{dr} - T_w) \tag{26}$$

where F_{dr} [m s^{-1}] is the flow of water entering the system per square metre of surface water. Of course, (26) requires the temperature of the drainage water to be measured or estimated. A practical way to estimate this temperature would probably be to equate it to the soil temperature at the depth where the drainage flow occurs. In case of surface runoff, this implies the assumption that the residence time of precipitation in the field is long enough to allow T_{dr} to become equal to the soil surface temperature.

2) *Advection*
Including an advection term as a source or sink term allows creating a quasi-2D approach in the present framework. This may be required, for example, in case of a ditch with flow velocity v [m s^{-1}]. Assuming well-mixed conditions and horizontal homogeneity in the control volume described by the 1D framework, as well as in the upstream neighbouring control volume, the impact of the upstream water on the control volume expressed as source term S_{adv} [W m^{-2}] is given by:

$$S_{adv} = \rho_w c_w h v (T_{w,up} - T_w) / \Delta x \tag{27}$$

where $T_{w,up}$ [K] is the temperature of the water advected from the upstream control volume and Δx [m] is the distance between the nodes of the upstream and downstream control volume where temperature difference $T_{w,up}$ - T_w is evaluated. Equation (27) should be evaluated for each control volume of the model grid.

3.2.7 Numerical implementation

Equation (1) can be solved using an explicit time stepping scheme, so that

$$T_w^i = T_w^{i-1} + \frac{\Delta t}{\rho_w c_w h}\left(K_d - K_u + L_d - L_u - H - \lambda E + G_s + Q_{pr} + \sum S\right) \tag{28}$$

in which the superscript denotes the timestep. Apart from considerations regarding sufficient numerical stability, the size of the timestep has to be chosen such that stationarity within the time step is a reasonable approximation. This implies that within a timestep the fluxes as well as water depth h in (28) may be assumed constant. The heat fluxes are usually considered (quasi-) stationary at timescales of 0.5 - 1 hour. This is probably also a reasonable timescale to assume stationarity for the sink and source terms S. Although h may vary quite strongly (Adriaanse and Beltman, 2009), a timestep of 10 minutes will ensure that in most cases the relative change in h will be small enough to assume a constant water depth within a timestep. Exceptions are water bodies of limited extent and with small water depth under conditions of large inflow of water, such as small water pools in case of intense precipitation. However, in such cases the validity of the present theoretical framework may be questioned. In some cases, a spinup time may be required, in order to allow equilibration between the water temperature and the meteorological conditions.

The temperature of the sediment can also be computed using an explicit scheme and the same timestep as in (28):

$$T_{sed}^i = T_{sed}^{i-1} + \frac{\Delta t}{\rho_w c_w D_{sed}}(G_{K\downarrow} + G_{gw} - G_s) \tag{29}$$

Alternatively, the diagnostic equation (20) may be used instead of (29).

3.2.8 Initial and boundary conditions

In the present framework, the following classes of initial and boundary conditions should be specified.

1. Model control, such as starting time, length of the timestep
2. General characteristics such as geographic location.
3. Physico-chemical properties of the water such as light absorption coefficients, emissivity and albedo.
4. Properties of the water body, such as depth, velocity of the water, orientation, and sediment albedo. This class also includes specification of initial water temperature T_w^0 (see equation 28).
5. Meteorological conditions such as air temperature, humidity and wind speed
6. Properties to describe interactions with the soil and surrounding fields, including the groundwater temperature, heat conductivity and roughness

Appendix 1 provides an overview of the required data and, if applicable, their possible sources. The list is ordered according to the aforementioned classes.

4 Sample calculations

4.1 General

In this chapter we present sample calculations with the proposed set of equations and parameterizations to compute water temperature in the TOXSWA model environment. The purpose of the chapter is to examine a number of important general characteristics of the system, and to investigate the effect of the improved temperature simulations on the degradation of PPP in small water bodies. The following main issues are addressed here:

- Performance of the system, using different datasets of meteorological drivers
- Sensitivity to light absorption coefficient and water depth.

The sample calculations were performed using the spreadsheet program Microsoft Excel®.

For evaluation purposes observations as well as results of simulations with a detailed 1D diffusion model were used. The diffusion model, VOC (Vertical Ocean Model; Large et al., 1994) is a research model that can be used to study air-water exchanges and properties of the water column of various types of water bodies. Originally, the VOC model has been designed to describe the upper part of deep oceans and air-sea exchanges. The model has subsequently been extended to simulate properties of coastal waters (Jacobs et al., 2002) and aquaculture ponds (Jacobs et al., 2009). The most recent model version is able to account for the physics described in Chapter 2, except for extreme boundary effects such as sloping sediments in very small ditches. The model has been successfully validated for an aquaculture pond in the open air, using water temperature and meteorological observations. It has been applied to describe the energy balance of aquaculture ponds and to assess requirements for the conditioning of such ponds to avoid temperature extremes. Together with observations, the VOC model can be used to study the limitations of the new modelling concept and in some cases also to calibrate the new bulk concept.

The effect of the various temperature time series on the degradation of PPP is evaluated by feeding the various temperature time series to the degradation function applied in TOXSWA. Degradation is assumed to follow pseudo first-order reaction kinetics. PPP concentration C is computed from

$$C_{i+1} = C_i \exp(-k_{i+1}\Delta t) \tag{30}$$

where k [s^{-1}] is the reaction rate constant, Δt [s] is the size of the timestep and subscript i indicates the timestep count. Thus, k is evaluated using the temperature of timestep $i+1$. The response of k to temperature T [°C] is computed as follows:

$$k(T) = k_{20} \exp\left(-\frac{E_a}{R^*}\left[\frac{1}{T+273.15} - \frac{1}{293.15} \right] \right) \tag{31}$$

where k_{20} is the value of k at a temperature of 20°C, E_a [kJ mol^{-1}] is the activation energy (65.4 kJ mol^{-1}; EFSA, 2007) and R^* [8.314 J K^{-1} mol^{-1}] is the universal gas constant.

4.2 Performance of the proposed bulk approach

4.2.1 Setup

The goal of our first set of temperature calculations with the proposed bulk model is an analysis of the performance regarding the simulated temperature. The results of the calculations are compared with observations and with results of simulations with the more detailed diffusion model VOC.

The observations used in the evaluation were performed at an open water body of 10m x 100m, with a mean water depth of 32 cm. Data are available for the period 24 June 2008 until 26 February 2009. In this period, incoming and reflected shortwave radiation, incoming and emitted longwave radiation, air temperature and humidity, wind speed and wind direction were observed over the water body. Furthermore, in the water PAR and temperature were observed. Precipitation and atmospheric pressure were obtained from a nearby weather station. Both the meteorological observations and the VOC model are discussed extensively in Jacobs et al. (2009).

In sample calculations of the present study we focus on a relatively warm period in the summer of 2008, 11 July - 10 Aug, with large temporal variations of the water temperature. In the selected period, the observed water temperature ranged between 13.8 and 29.1 °C, with an average of 21.3 °C. The observed daily amplitude ranged between 2.4 °C and 8.2 °C, with an average of 5.1 °C. In the same period, the air temperature at 1.3 m above the surface of the water body varied between 10.9 °C and 27.5 °C, with an average of 18.0 °C.

Three sets of calculations were performed with the bulk model, all in a strictly 1-D mode (that is, no lateral influences):

1. using the meteorological conditions observed directly over the water body. Results of this simulation will serve to assess the potential, physical performance of the model, that is, the performance with near-optimal availability of observations of driving variables: incoming shortwave and longwave radiation, wind speed, air temperature and humidity. Air pressure and precipitation are according to the observations at the meteorological station 'Wilhelminadorp', made available by the Royal Netherlands Meteorological Institute (KNMI). Henceforth this case will be labelled SIM1.
2. using a set of standard meteorological observations in De Bilt, the location of the main KNMI meteorological station in the centre of the Netherlands. This represents a more realistic case where the TOXSWA simulations utilize meteorological data gathered at a somewhat distant location. Comparison with SIM1 allows an assessment of the possible degradation of the performance caused by application of such a suboptimal set of meteorological data. Both incoming shortwave and incoming longwave radiation are not commonly available in standard reports from meteorological stations. Therefore, they must be estimated from Eqs. (2)-(4) for shortwave radiation and Eqs. (11)-(12) for longwave radiation, using the observed air temperature, humidity and cloud cover along with the geographic location. This case will be labelled SIM2.
3. using the meteorological observations from De Bilt, but now including observed incoming shortwave radiation. This case is labelled SIM3. It is similar to SIM2, the only difference being that observed incoming solar radiation is used instead of computing it from parameterization (2)-(4). This case is added because recently, hourly observations of incoming solar radiation have become available as standard output from the meteorological stations in the Netherlands. The possible improvement of the performance when using these data instead of the parameterization is assessed.

In most cases, we used radiation attenuation coefficients determined by Jacobs et al. (2009) from observations in an aquaculture pond (Table 3.1). Because the results sometimes showed a systematic deviation from the observations, we performed some additional simulations using the default values that represent a fit

to the modelled light absorption characteristics described by Jacobs et al. (2008). These additional simulations will be labelled with '*a*' (for example, SIM1a).

The sediment temperature was chosen to be equal to the soil temperature observed at 50 cm depth in a grass-covered clay soil in Wageningen in the same period. These data are available from: www.met.wau.nl/haarwegdata This method was found to give the best results with VOC, although the differences with their dynamic simulations were small (Jacobs et al., 2009).

The VOC model was run for the same period, using meteorological data obtained directly over the water body (cf. first set of calculations). These simulations provided the model reference case for our evaluation. Both the sample calculations with the bulk approach and the reference run with VOC used a time step of 3600 s, which is larger than the one envisaged for the TOXSWA application (900 s or less), and also larger than the timestep of 900 s used by Jacobs at al. (2009) in their simulations with VOC. However, this time step was chosen because it equals the time interval of one hour from the weather station reports. Variations in the meteorological drivers faster than 1 hour are therefore not captured.

4.2.2 Results and discussion

Figure 4.1 depicts the observed and simulated water temperature for SIM1, SIM2, SIM3, and for the reference run with VOC. For VOC the temperature was taken halfway the water column, at a depth of 16 cm below the water surface.

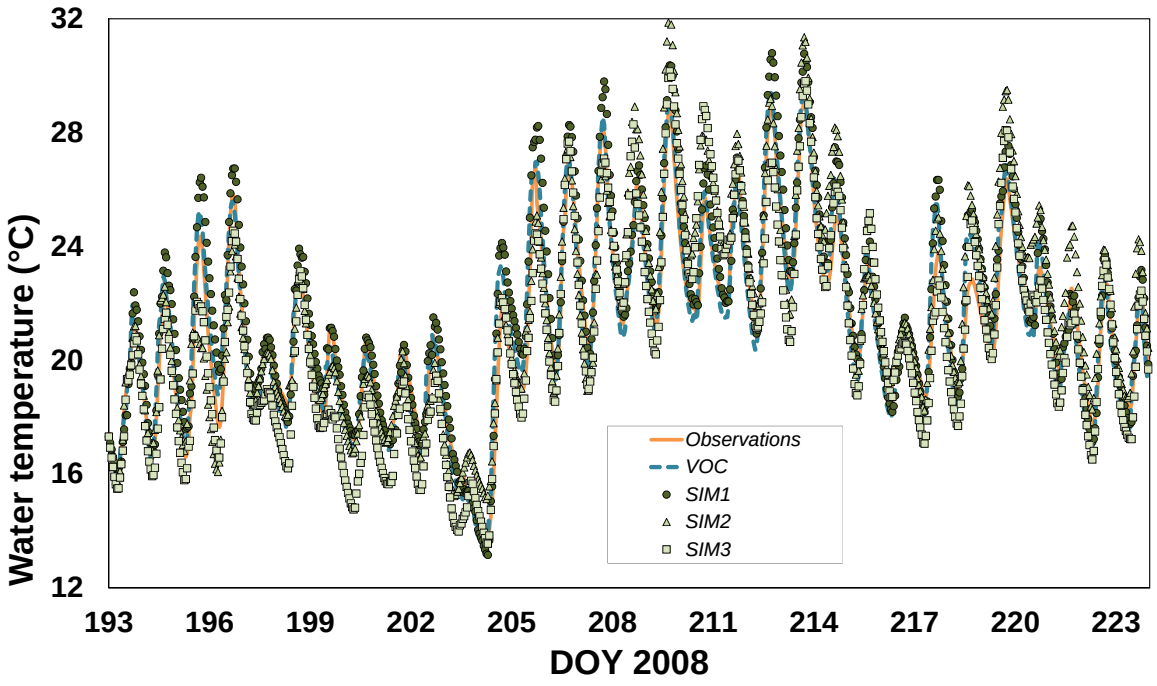

Figure 4.1

Water temperature simulations using the bulk approach (SIM1, SIM2 and SIM3) and comparison with observations and simulations with the detailed VOC model. In all cases the water depth is 32 cm. SIM1 and VOC use observations of radiation, air temperature and humidity and wind speed obtained directly at the water body; SIM2 uses wind speed, air temperature and humidity from standard meteorological observations in De Bilt (Netherlands) and estimates the radiation fluxes from these observations and the reported total cloud cover; SIM3 is similar to SIM2 but uses observed incoming solar radiation from De Bilt. See main text for further explanation.

It can be seen that the trends in the water temperature simulated in the runs with the bulk system are quite similar and compare reasonably well with the observations as well as with VOC calculations. The main features at hourly to monthly timescales seem to be captured reasonably well. However, there is a slight tendency to overestimate the maximum temperatures. In some cases, the minimum temperature is underestimated. Thus, the amplitude is somewhat larger than observed. But this tendency is also present in the VOC simulations, and should therefore not be interpreted as a shortcoming of the bulk system *per se*.

Table 4.1 summarizes the performance of the sample calculations in the various cases along with the performance of the VOC reference run. Four performance indicators are listed: the *bias* (average deviation between model and observation), *RMSE* (root of the mean squared error), *%hit* (fraction of the simulated temperatures within 1 K from the observations), and correlation r^2. All indicators are evaluated on an hourly basis.

It can be seen that the VOC model outperformed the simulations with the bulk model. All indicators show better performance, except for the correlation coefficient r^2, which was slightly lower than the one for SIM1. However, the indicators confirm the impression from Figure 4.1 that the performance of the bulk model is quite acceptable. For VOC and SIM1 it was investigated whether some further improvement could be obtained by using a smaller time step. The observations available for each half hour were interpolated to 6-min intervals instead of using hourly value as in the original setup. Reducing the timestep to 6 minutes noticeably improved the performance of VOC, but hardly improved the results of SIM1 (not shown).

Comparison between SIM1 and SIM2 reveals that, as expected, using the standard observations from the centre of The Netherlands reduces the quality of the simulations with the bulk system. However, it is assessed that the comparison presented here may represent a 'worst case', since the observations at the pond were obtained near the coast of the country. It is well known that the weather near the coast of the Netherlands may differ considerably from the weather observed in De Bilt (Heijboer and Nellestijn, 2002). For example, on day 195 it was quite cloudy in De Bilt, but sunny over the pond near the coast. For this reason both SIM2 and SIM3 clearly underestimated the water temperature for that day. In spite of such inevitable differences in driving variables, the simulations with observations from De Bilt are quite acceptable with a hit percentage of over 50. Using observations from a more nearby weather station could further improve the simulations.

Interestingly, using the observed solar radiation in De Bilt instead of the estimated one did not clearly improve the quality of the bulk simulations. Although *RMSE* and r^2 were slightly better, the bias became negative with an absolute value about equal to the one of SIM2. As a result the %hit reduces somewhat. Possibly, the quality of the simulations would benefit from using the observed solar radiation if meteorological data from a nearby station would be used.

As was already noted before, SIM1 and SIM2 clearly revealed a positive bias. Therefore, it was also investigated whether setting the absorption coefficient for PAR to its lower default value (2.52 m^{-1}, see Table 3.1) improved the performance of the bulk simulations. An additional run with VOC using this value was carried out as well. The lower default value would arguably be more appropriate for moderately clear water. Although no light absorption values were reported for the selected period by Jacobs et al. (2009), the lower absorption reported for the second half of August suggests that the water may have been less turbid in July and the first half of August than was assumed in the previous simulation.

The performance of the additional calculations with the lower absorption coefficient is shown in Table 4.2. It can be seen that SIM1a as well as SIM2a perform significantly better than SIM1 and SIM2, respectively. Bias and RMSE both decrease, while *%hit* and r^2 increase. In particular the SIM1a simulations show a large improvement relative to SIM1. By contrast, the VOCa and SIM3a performances are clearly worse than their counterparts with the higher attenuation coefficient.

Based on this result in combination with the fact that the deviations tend to increase in daylight conditions and decrease during the night, we presume that the bias is related to ignoring the thermal stratification due to light absorption. The latter characteristic of the present bulk model results in underestimation of the surface tempera- ture during the day.

Table 4.1

Performance of VOC, SIM1, SIM2 and SIM3 in terms of bias, RMSE, %hit and r^2, using the value of the PAR absorption coefficient optimized for VOC (4.25 m^{-1}, see Jacobs et al., 2009). The optimization was based on observations.

	VOC	SIM1	SIM2	SIM3
Bias	0.022	0.640	0.472	-0.432
RMSE	0.767	1.067	1.432	1.310
%hit	87.5	67.2	54.4	52.8
r^2	0.945	0.955	0.868	0.897

Table 4.2

Performance of VOCa, SIM1a, SIM2a and SIM3a in terms of bias, RMSE, %hit and r^2, using a value of the PAR absorption coefficient of 2.52 m^{-1}. This value represents a fit to the light absorption characteristics used by Jacobs et al. (2008).

	VOCa	SIM1a	SIM2a	SIM3a
Bias	-0.732	0.008	-0.121	-1.071
RMSE	0.961	0.644	1.272	1.562
%hit	61.2	90.3	60.2	39.0
r^2	0.956	0.963	0.859	0.892

Hence, the loss of energy by radiative and turbulent exchange is underestimated. The temperature rise is therefore too strong during the day, and is, in the period investigated here, not fully compensated by enhanced energy loss during the night. Introducing a stability indicator in combination with a surface temperature correction may repair this problem. However, finding an approach suitable for implementation in TOXSWA needs some further analysis and investigation.

Finally, degradation of PPP in water was assessed for each of the calculation methods. The degradation was computed using (30)-(31) with the simulated temperatures from VOC/VOCa, SIM1/SIM1a and SIM2/SIM2a or the hourly observed temperatures (OBS). We also performed calculations using the monthly averaged observed water temperature in the simulation period ($T_{w,av}$). In all cases, the degradation was assessed for a PPP with extremely fast degradation, with DT50 = 0.25 day (6 hours at 20°C, assuming an energy of activation of 65.4 kJ mol^{-1}; EFSA, 2007). At the start of each day, the remaining fraction was reset to 1. For the more realistic temperature time series, the remaining fraction at the end of each day will vary in the course of the month, because of the temperature fluctuations.

Figure 4.2 shows the remaining PPP fraction averaged over the 30 days of the simulation. Using the observed water temperature and their fluctuations, the average remaining fraction is 5.54%. Results from VOC and SIM1a are quite close to that: 5.50% and 5.56%, respectively, whereas results for SIM1 (4.79%) and VOCa (6.55%) clearly deviate more.

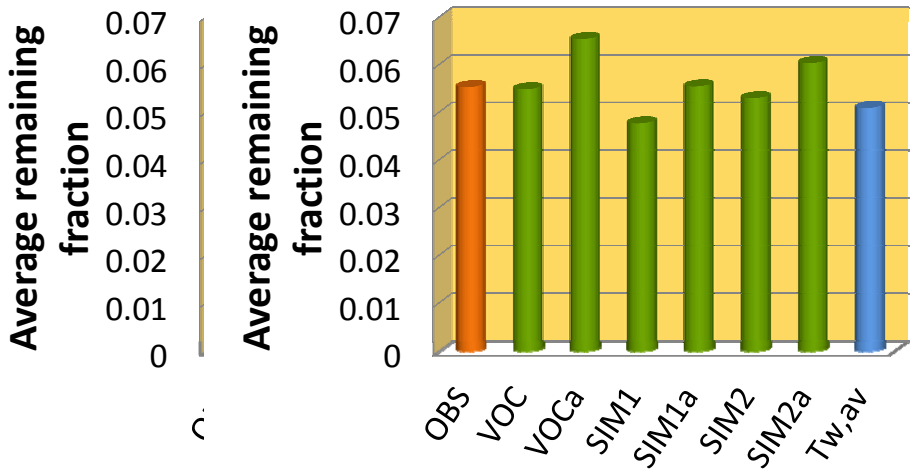

Figure 4.2

Average (n=30) remaining fraction after one day for a PPP with a half-life at 20°C of 0.25 day. The fractions were assessed with (30)-(31), using the various water temperature time series discussed in the text. At the start of each day the remaining fraction were reset to 1.

The deviations from the various runs are predominantly related to the mean bias. However, there is also a small but clear effect of diurnal temperature variations: using the average observed water temperature (case 'Tw,av') gives an average remaining fraction of 5.11%, approximately 8% lower than the one obtained with the fluctuating observed temperature.

The possible variation of PPP degradation within a month is illustrated in Figure 4.3, where the daily remaining fraction during the simulation period is shown. The results for OBS and Tw,av are compared with SIM1a, VOCa and SIM1. The latter cases have been chosen because they represent the run with smallest bias (SIM1a), the largest negative bias (SIM1) and the largest positive bias (VOC1) of the cases considered in Figure 4.2. Clearly, using the monthly average would significantly underestimate the remaining fraction during Day 1-12, and overestimate it during Day 13-22. The behavior at timescales shorter than a month may be important when evaluating application scenarios for PPP. Using a reasonably accurate model to predict water temperatures has a clear advantage is such cases. For the cases shown here, even the worst model simulations give much better information than can be obtained when using the average air temperature.

In general, even though the advantages of estimates based on the bulk system model over using a monthly average temperature may seem limited, one should consider that in the current TOXSWA procedure the average water temperature is derived from air temperatures. This introduces a considerable amount of uncertainty that may be reduced significantly by application of the estimation procedures based on the bulk approach.

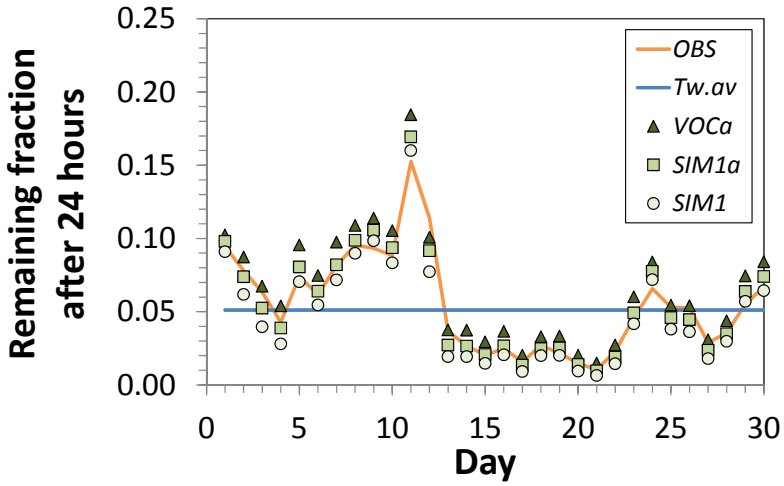

Figure 4.3

Remaining fraction after one day for a PPP with a half-life at 20°C of 0.25 day. The fractions were assessed with (30)-(31), using the various water temperature time series discussed in the text. At the start of each day the remaining fraction was reset to 1.

4.3 Effect of water depth and light attenuation

4.3.1 Setup

The goal of our second set of sample calculations with the proposed bulk model is a first assessment of the effects of water depth and light attenuation on the water temperature and resulting PPP degradation. Only the VOC model was used as a reference, since the observations used to evaluate the bulk model (Section 4.2) are valid only for the specific case of a water depth of 32 cm. However, we focussed on the same period in the year 2008.

It is important to realize that turbidity or light attenuation and depth need not be independent. Phytoplankton growth is limited by light, amongst other factors. The phytoplankton population will increase as long as the light intensity is sufficient to sustain growth. However, due to the increasing light attenuation by the growing phytoplankton population, available light will become limiting and mortality will balance growth. This point is reached at a given degree of light absorption. The amount of phytoplankton that can be sustained depends on this maximum degree of light absorption and is independent of depth. For the case of well mixed water, this implies that the light attenuation coefficient must be inversely proportional to depth. That is, all other factors being equal, shallow water will become more turbid than deep water when sustaining the same optimum amount of phytoplankton biomass.

Based on the reasoning given above, sample calculations were performed for a shallow water of depth h = 0.16 m and a somewhat deeper water of depth h = 1.28 m. The light attenuation coefficient was derived from the measurements by Jacobs et al. (2009). Thus, μ = 8.5 m^{-1} for h = 0.16 m and μ = 1.06 m^{-1} for h = 1.28 m. However, in some cases where the water quality is dominated by physico-chemical influences rather than by biological mechanisms, a constant absorption coefficient may be more appropriate. Therefore, calculations were performed where μ was independent of h. In these calculations μ was set to the values given in Table 3.1, that is, μ = 4.25 m^{-1} or μ = 2.52 m^{-1}, respectively.

In summary, sample calculations were performed with:

- h = 0.16 m, μ = 8.50 or 4.25 or 2.52 m^{-1}
- h = 1.28 m, μ = 4.25 or 2.52 or 1.06 m^{-1}

All simulations were carried out with the proposed bulk system (SIM1) as well as with the detailed diffusion model (VOC). The meteorological conditions observed directly over the water body were used to drive the models. Again, the sediment temperature was chosen to be equal to the soil temperature observed at 50 cm depth in a grass-covered clay soil in Wageningen in the same period. Moreover, all sample calculations use a time step of 3600 s.

The sensitivity of simulated degradation of PPP in water to choosing one of the calculations methods was assessed, using (30)-(31) with the simulated temperatures from SIM1 and VOC, respectively. Again, the remaining fraction after 24 hours was evaluated for a PPP with *DT50* = 0.25 day, while resetting the fraction to 1 at the start of each day.

4.3.2 Results and discussion

Figure 4.4 shows the simulated average water temperature (left) along with the average remaining PPP fraction after one day (right) for the various light attenuation coefficients and depths. Comparison of T_w and the average remaining fraction confirms that the average remaining fraction is mainly driven by the average water temperature. It can be seen that the bulk system generally yields higher temperatures and therefore somewhat lower remaining fractions than VOC. In particular the differences at a water depth of 0.16 m are considerable. This is consistent with the results presented in Section 4.2. Note that the trends are similar for both depths.

The fact that differences are much less at the larger water depth indicates that they are most probably related to temperature differences caused by absorption of light. The difference may be resolved by introducing an indicator for stability in the upper water layers, in combination with a correction for temperature differences near the water surface. This is beyond the scope of the present study, but could be a subject for future developments of the TOXSWA system.

It can be seen that the average temperature (remaining fraction) increases (decreases) with increasing μ at a water depth of 0.16 m, but the effect seems to level off at a depth of 1.28 m. This can be explained as follows.

At a given value of μ the total absorption in case of lower water depth will be lower than in the case of the larger water depth. In well mixed water the maximum temperature is related to the maximum amount of radiation that can be absorbed. Since the total amount of solar radiation that can potentially be absorbed depends on the weather only, the maximum absorption is reached at much lower values of μ in the case of the deeper water. Increasing the attenuation coefficient does not further in- rease the total absorption anymore. Similarly, if the absorption coefficient is inversely proportional to depth, the total amount of solar radiation absorbed will be about equal for all water depth. Thus, the temperature and therefore the decay will be about equal for well mixed water. This can clearly be seen by comparing the results for μ = 1.06 m^{-1} and μ = 8.50 m^{-1}. The assumption that μ = f(h) renders the results almost insensitive to h and μ.

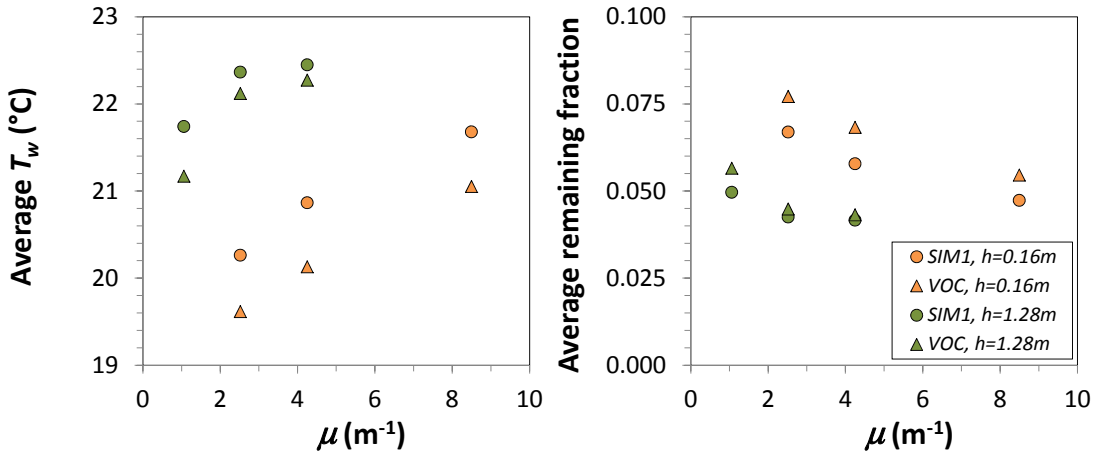

Figure 4.4

Average (n=30 days) water temperature (left) and remaining PPP fraction after 24 hours (right) as a function of the PAR attenuation coefficient and at h = 0.16 or 1.28 m, respectively. Bulk system simulations are indicated with SIM1, simulations with the detailed diffusion model with VOC.

Apart from the averages shown in Figure 4.4 the diurnal variation of the temperature may be important, since this also determines the variation of PPP degradation. This can clearly be seen in Figure 4.5, where the simulated hourly temperature is shown in the upper panel and the corresponding remaining PPP fraction for each day in the lower panel. A greater water depth dampens the temperature fluctuations and extremes occur somewhat later than at shallow water depth. Both features are evident in Figure 4.5, both for the temperature time series and for the PPP decay time series. Such differences may be quite important when evaluating PPP application scenarios. Note that the bias of SIM1 relative to VOC is also clearly visible.

Results with μ independent of depth were largely similar to the ones shown in Figure 4.5. Nevertheless, there were some noticeable differences. The resulting time series are not shown individually, but the temperature dynamics of the various cases are summarized in Figure 4.6. The diagram shows the characteristics of the daily amplitude, defined as the difference between the minimum and the maximum water temperature on a particular day. The filled circles represent the average (n=30 days) amplitude, while the arrows indicate the modelled amplitude range.

The figure once again demonstrates the much smaller amplitude and amplitude range for deeper water. Also, for the lower water depth there is a clear impact of the radiation attenuation coefficient (turbidity) on the amplitude. Both the average value and the range of the temperature amplitude are affected.

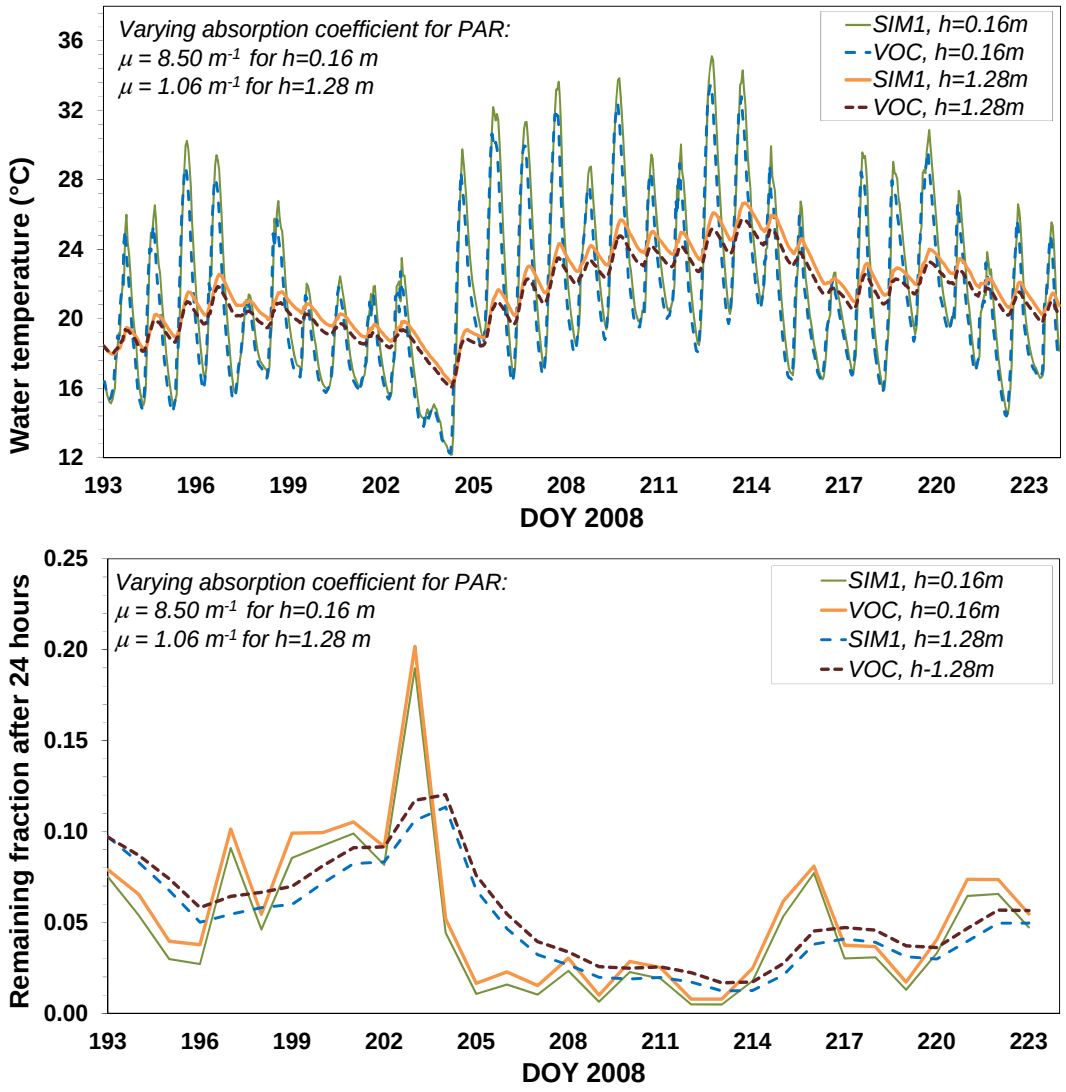

Figure 4.5

Simulated water temperature (upper panel) and corresponding remaining PPP fraction after 24 hours for a water depth of 0.16m and 1.28m, respectively. Absorption coefficient μ was taken to be a function of depth in these cases.

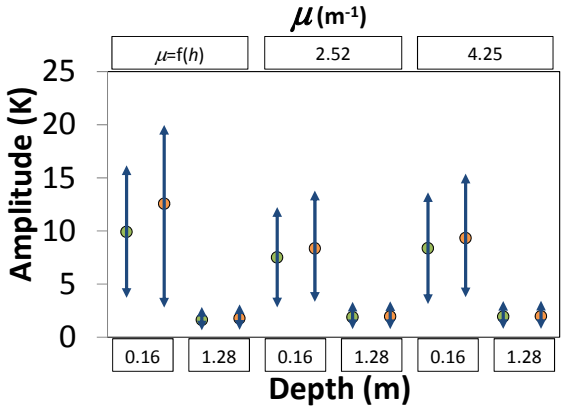

Figure 4.6

Daily amplitude of the modelled water temperature as a function of depth (lower axis) as well as PAR absorption coefficient (upper axis). Averages are denoted by the circles (n=30 days). The range of the amplitudes is indicated by means of the arrows.

The variation is much larger for the higher turbidity. For μ = f(h), which means μ = 8.50m^{-1} in the case of h=0.16m, the modelled SIM1 amplitude varies between 2.8 and 20.0 K, with an average of 12.6 K, whereas for μ = 2.52 m^{-1} the amplitude varies between 3.3 and 13.8 K, with an average of 8.4 K. For VOC, the pattern is similar, though somewhat less extreme.

These results confirm that turbid shallow water is an extremely dynamic system with regard to water temperature. Such systems may benefit the most from physically realistic temperature estimates for the calculation of degradation rates of PPP.

5 Conclusions and recommendations

A reasonable estimate of the water temperature is needed in order to get a good description of the degradation of plant protection products (PPP) in water, such as required by the TOXSWA model. Since natural water bodies are strongly influenced by weather conditions that vary at timescales down to one hour, a proper description of the response of water temperature to the weather conditions is required.

We suggest designing a 1D-bulk model for simulation of the thermal behaviour of water bodies for use in TOXSWA. Such a model captures the main physical features of the energy balance of open water, has limited data requirements or data can be easily obtained, and would fit well in the present TOXSWA environment. Moreover, it can be easily extended into a quasi 2-D approach that allows inclusion of several lateral influences on the water temperature.

However, the proposed modelling system has the following main limitations:
(i) thermal stratification cannot be handled
(ii) the light absorption model will not necessarily be valid for systems where macrophytes dominate light absorption
(iii) the possible influence of walls on radiation exchange is not taken into account
(iv) cases where horizontal exchange is exceptionally large in comparison with the vertical exchange may not be adequately described
(v) freezing of water and melting of ice are not modelled

Future developments of the TOXSWA system to estimate water temperatures may need to consider these factors as well.

Results from sample calculations show that the proposed bulk system is able to capture the main features at hourly to monthly timescale well or reasonably well, depending on the quality of the available meteorological data. However, there is a tendency to overestimate the maximum temperatures, resulting in a positive bias. It is assessed that the tendency for positive bias is related to ignoring the thermal stratification due to light absorption. Introducing a stability or density stratification indicator in combination with a surface temperature correction may repair this problem. However, finding an approach suitable for implementation in TOXSWA is beyond the scope of the present study and needs further analyses and investigation.

Sample calculations demonstrating the sensitivity to depth in combination with light attenuation are presented as well. Results from the proposed bulk system were compared with results from simulations with a detailed 1D diffusion model, using meteorological conditions observed directly over the water body to drive the models.

In natural waters where light attenuation is inversely proportional to depth, the monthly average temperature will be rather insensitive to water depth, because of compensating effects of light attenuation. However, if light attenuation is independent of depth, the monthly averaged temperature and daily maxima increase with increasing turbidity (more light attenuation) until all available solar energy is being absorbed. For deep water, this natural maximum light absorption is reached at less turbid conditions than for shallow water, due to the longer light path-length in the former case.

Estimates of the degradation of a PPP with a half-life of 0.25 day at 20 °C, using the various temperature time series from observations and sample calculations, remained within 18% from the estimates using observed temperature. The results confirm that the average remaining PPP fraction is correlated with mean temperature, so that bias will significantly influence deviations from calculations based on observed temperature. However, for the period investigated here the effect of diurnal temperature variations was estimated to be about 8%. The main advantage in using temperature variations at the time scale of one hour is that degradation dynamics of short-lived PPP can be included, which is needed for evaluation of application scenarios. In particular evaluation of PPP degradation in shallow, highly turbid waters may benefit from improved temperature estimates at sub-daily timescale.

References

Adriaanse, P.I. and W.H.J. Beltman, 2009. *Transient water flow in the TOXSWA model (FOCUS versions): concepts and mathematical description.* Wageningen, Statutory Research Tasks Unit for Nature and the Environment. WOt-report No. 101.

Arya, S.P., 2001. *Introduction to micrometeorology*. Academic Press, San Diego.

Bindi, M., F. Miglietta and G. Zipoli, 1992. Different methods for separating diffuse and direct components of solar radiation and their application in crop growth models. *Clim. Res.*, 2, 47-54.

Brutsaert, W., 1982. *Evaporation into the atmosphere.* Kluwer Academic Publishers, Dordrecht, 299 pp.
Cathcart, T.P., 1987. *Heat transfer and temperature prediction in small freshwater ponds.* Ph.D. thesis, Univ. Mariland, Dept. Agricultural Engineering, 299 pp.

Csanady, G.T., 1990, The role of breaking wavelets in air-sea gas transfer. *J. Geophys. Res.***,** 95, 749-759.

DeCosmo, J., K.B. Katsaros, S.D. Smith, R.J. Anderson, W.A. Oost, K. Bumke and H. Chadwick, 1996. Air-sea exchange of water vapor and sensible heat: The Humidity Exchange Over the Sea (HEXOS) results. *J. Geophys. Res.*, 101, 12001-12016.

Deneer, J.W., W.H.J. Beltman and P.I. Adriaanse, 2010. *Transformation reactions in TOXSWA.* Alterra report 2074. Alterra, Wageningen, The Netherlands.

EFSA, 2007. Opinion on a request from EFSA related to the default Q10 value used to describe the temperature effect on transformation rates of pesticides in soil. Scientific opinion of the panel on plant protection products and their residues. *The EFSA Journal* 622, 1-32.

Erbs, D.G., S.A. Klein and J.A. Duffie, 1982. Estimation of the diffuse radiation fraction for hourly, daily and monthly-averge global radiation. *Solar Energy*, 28, 293-302.

Foken, T., 2008. *Micrometeorology*. Springer Verlag, Berlijn, Heidelberg.

Garratt, J.R., 1992. *The atmospheric boundary layer*. Cambridge University Press, Cambridge.

Graham Cogley, J., 1979. The albedo of water as a function of latitude. *Monthly. Weather Rev.*, 107, 775-781.

Gill, A.E., 1982. *Atmosphere-Ocean dynamics.* Academic Press, San Diego, 662 pp.

Heijboer, D. and J. Nellestijn, 2002. *Klimaatatlas van Nederland; de Normaalperiode 1971-2000.* Elmar B.V., Rijswijk, the Netherlands, 182 pp. (Dutch Text).

Holtslag, A.A.M. and A.P. van Ulden, 1983. A simple scheme for daytime estimates of the surface fluxes from routine weather data. *J. Climate Appl. Meteor.*, 22**,** 517-529.

Hull, J.R., K.V. Liu, W.T. Sha, J. Kamal and C.E. Nielsen, 1984. Dependence of ground heat loss upon solar pond size and perimeter insulation. *Solar Energy*, 33, 25-33.

Jacobs, A.F.G., B.G. Heusinkveld, A. Kraai and K.P. Paaijmans, 2008. Diurnal temperature fluctuations in an artificial small shallow water body. *Int. J. Biometeorol.*, 52, 271-280, doi: 10,1007/s00484-007-0121-8.

Jacobs, C.M.J., J.F. Kjeld, P.D. Nightingale, R.C. Upstill-Goddard, S.E. Larsen and W.A. Oost, 2002. Possible errors in CO2 air-sea transfer velocity from deliberate tracer releases and eddy covariance measurements due to near-surface concentration gradients. *J. Geophys. Res.* C9, 107, 11-1 to 11-26, doi:10,1029/2001JC000983.

Jacobs, C.M.J, H.W. ter Maat, J.A. Elbers and L.C.P.M. Stuyt 2009. *Conditionering van de Watertemperatuur in Buitenvijvers voor de Aquacultuur*. Wageningen, Alterra, Alterra-Report, Confidential (Dutch text).

Katsaros, K.B., 1980, The aqueous thermal boundary layer*. Boundary-Layer Meteorol.*, 18, 107-127.

Kraus, E.B. and J.A. Businger, 1994. *Atmosphere-ocean interaction*. Oxford University Press, New York, 363 pp.

Lamoureux, J., T.R. Tiersch, S.G. Hall, 2006. Pond heat and temperature regulation (PHATR): Modeling temperature and energy balances in earthen outdoor aquaculture ponds. *Aquacultural Engineering* 34, 103-116.

Large, W. G., J. C. McWilliams and S. C. Doney, 1994. Oceanic vertical mixing: A review and a model with a nonlocal boundary layer parameterization*. Rev. Geophys*. (32), 364-403.

Losordo, T.M. and R.H. Piedrahita, 1991. Modelling temperature variation and thermal stratification in shallow aquaculture ponds. *Ecological Modelling*, 54, 189-226.

Monteith, J.L. and M.H. Unsworth, 1990, *Principles of environmental physics*. Edward Arnold, Londen.

Paaijmans, K.P., B.G. Heusinkveld and A.F.G. Jacobs, 2008a. A simplified model to predict diurnal water temperature dynamics in a shallow tropical water pool. *Int. J. Biometeorol.*, 52, 797-803.

Paaijmans, K.P., A.F.G. Jacobs, W. Takken, B.G. Heusinkveld, A.K. Githeko, M. Dicke and A.A.M. Holtslag, 2008b. Observations and model estimates of diurnal water temperature dynamics in mosquito breeding sites in western Kenya. *Hydrological Processes*, 22, 4789-4801.

Paulson, C.A. and J.J. Simpson, 1977. Irradiance measurements in the upper ocean. *J. Phys. Oceanogr.*, **7**, 952-956.

Reynolds, C.S., A.E. Irish and J.A. Elliott, 2001. The ecological basis for phytoplankton responses to environmental change (PROTECH). *Ecological Modelling* 140, 271-291.

Rooy, W.C. de and A.A.M. Holtslag, 1999. Estimation of Surface Radiation and Energy Flux Densities from Single-Level Weather Data. *J. Appl. Met.,* 38, 526-540,

Scheffer, M., 2004. *Ecology of shallow lakes* (3rd edition). Kluwer Academic Publishers, Dordrecht, 357 pp.

Stull, R.B., 1988. *An introduction to boundary layer meteorology*. Kluwer Academic Publishers, Dordrecht, Boston, London.
Terray, E.A., M.A. Donalan, Y.C. Agrawal, W.M. Drennan, K.K. Kahma, A.J. Williams III, P.A. Hwang and S.A. Kitaigorodskii, 1996. Estimates of kinetic energy dissipation under breaking waves. *J. Phys. Ocean.*, 26, 792-807.

Troen, I.B. and L. Mahrt, 1986. A simple model of the atmospheric boundary layer. *Boundary-Layer Meteorol.*, 37, 129-148.

Appendix 1

In this appendix, an overview is given of the input data and boundary conditions required to run the bulk model. In the Table presented here, the following information can be found:

Column 1: Lists the symbols of the variables used in this report as far as applicable
Column 2: Gives the units of the listed variables
Column 3: Refers to the equation or equations where the variable appears
Column 4: Shortly describes the purpose of the variable
Column 5: Denotes the variable class. In the present framework, the following classes of initial and boundary conditions should be specified:

1. Model control, such as starting time, length of the time step.
2. General characteristics such as geographic location.
3. Physico-chemical properties of the water such as light absorption coefficients, emissivity and albedo.
4. Properties of the water body, such as depth, velocity of the water, orientation, and sediment albedo. This class also includes specification of initial water temperature T_w^0 (see equation 28).
5. Meteorological conditions such as air temperature, humidity and wind speed.
6. Properties to describe interactions with the soil and surrounding fields, including the groundwater temperature, heat conductivity and roughness.

Column 6: Lists the preferred data source. Sometimes, data values are available from observations; in other cases they should be computed; in yet other cases a default value can be specified.
Column 7: Alternative source. If the values for the variables cannot be taken from the preferred source, this alternative source could be used.
Column 8: Recommended default values.
Column 9: Some remarks. Also indicates whether or not a variable should be specified as a time series.

Note that in some cases, different data serve the same purpose and should be selected according to their availability. For example, if K_d and L_d are available from observations, their computation and therefore N and N_h are not required anymore.

Input	Unit	Equation	Purpose	Class	Preferred Source	Alternative source	Recommended default value	Remarks
n	-	9,10	number of wavelength bands in sunlight	3			2	Distinguish PAR and NIR; use more bands for purposes other than energy balance calculations
ξ_1	-	9,10	energy fraction in PAR	3			0.55	
ξ_2	-	9,10	energy fraction in NIR	3			0.45	
μ_1	m^{-1}	9,10	absorption coefficient in water for PAR	3	Observations	default value	$0.81/h$	Preferably h<2m; 46% of PAR and 75% of PAR+NIR reaches the sediment for all depths; can also be used for
μ_2	m^{-1}	9,10	absorption coefficient in water for NIR	3			1000	Keeps all NIR within first mm from the surface
ε_w	-	13	emissivity of water, compute L_u	3			0.97	Can be used for calibration
α_b	-	9b, 10	albedo of sediment, compute reflected K_d	4			0.3	
h	m	several	depth of the water column	4	TOXSWA			
w,r	m	correction	width, radius of water body, used in correction of G_s	4	TOXSWA			
v	$m\ s^{-1}$	27	bulk flow velocity	4	TOXSWA	default value	0-1	Default depends on conditions and type of water body
K_d	$W\ m^{-2}$	-	incoming shortwave radiation, boundary condition	5	Observations	equations 3,4		Timeseries
L_d	$W\ m^{-2}$	-	incoming longwave radiation, boundary condition	5	Observations	equation 11		Timeseries
u_r	$m\ s^{-1}$	14,15	wind speed at reference level, boundary condition	5	Observations	default values	(daily) climatological mean	Timeseries, compute from u_{obs} using (16) if $z_{obs} \neq z_r$
Tr	K	14,15,18,25	temperature at reference level, boundary condition	5	Observations	default values	(daily) climatological mean	Timeseries
H_r	-	15,25	relative humidity at reference level, boundary condition	5	Observations	default values	(daily) climatological mean	Timeseries, should be consistent with T_r
P_I	$m\ s^{-1}$	24	rain rate, boundary condition	5	Observations	default value	0	Timeseries, contribution is generally small

Input	Unit	Equation	Purpose	Class	Preferred Source	Alternative source	Recommended default value	Remarks
Start time	Year, month, day, hour	-	start of simulation, used for various purposes	1				
End time	Year, month, day, hour	-	end of simulation	1				
Spinup tim	days	-	Allow equilibration of Tw with meteorological conditions	1			3	Day 1 is repeated three times before the actual timestepping begins
Timestep	s	-	Timestepping	1			3600	Should be smaller in cases of strong variations in h; can be matched to TOXSWA timestep
Latitude	Degrees	2	specifies location, compute K_d	2			52	Default value for central Netherlands
Longitude	Degrees	2	specifies location, compute K_d	2			4	Default value for central Netherlands
a_1	W m^{-2}	3	turbidity factor, compute K_d	2			1041	Default value for central Netherlands
a_2	W m^{-2}	3	turbidity factor, compute K_d	2			-69	Default value for central Netherlands
b_1	-	4	cloud contribution factor, compute K_d	2			-0.75	Default value for Western Europe
b_2	-	4	cloud contribution factor, compute K_d	2			3.4	Default value for Western Europe
c_1	W m^{-2}	-	cloud contribution factor, compute L_d	2			70	
c_2	W m^{-2}	-	cloud contribution factor, compute L_d	2			50	
z_r	m	-	reference level for specification of meteorological boundary conditions	2			1.5	Height of screen level observations
α_t	-	-	albedo of water, compute reflected Kd	3	equation 5	default value	0.1	
α_{dir}	-	5	albedo of water for direct radiation, compute at	3	equation 6			
α_{dif}	-	5	albedo of water for diffuse radiation, compute at	3			0.06	Can be used for calibration

Input	Unit	Equation	Purpose	Class	Preferred Source	Alternative source	Recommended default value	Remarks
Pa	Pa	several	atmospheric pressure, various purposes, boundary condition	5	Observations	default value	101325	Timeseries, default is standard pressure
N	-	4,11	cloud cover fraction, boundary condition if K_d or L_d must be computed	5	Observations	default values	(daily) climatological mean	Timeseries
N_h	-	11	middle and low cloud cover fraction, boundary condition if K_d or L_d must be computed	5	Observations	default value	1	Timeseries
D_{sed}	m	19,21,28	depth of the sediment layer	1,6				Also serves as specification of model layout
T_gw	K	23	groundwater temperature, used to compute heat exchange with sediment	6	Observations	default value	long-term climatological mean of air temperature	Timeseries
T_{amp}	K	20	amplitude of the annual temperature wave, used in diagnostic computation of T_{sed}	6	Observations of soil temperature at sediment depth			Optimize to reproduce observations of soil temperature at depth of sediment, or use observations as timeseries of T_{sed}
D_{damp}	m	20	damping depth, used in diagnostic computation of T_{sed}	6	Observations of soil temperature at sediment depth			Optimize to reproduce observations of soil temperature at depth of sediment, or use observations as timeseries of T_{sed}
ϑ	rad	20	phase shift of temperature wave, used in diagnostic computation of T_{sed}	6	Observations of soil temperature at sediment depth			Optimize to reproduce observations of soil temperature at depth of sediment, or use observations as timeseries of T_{sed}
k_{sed}	W m^{-1} K^{-1}	19	heat conductivity of the sediment, compute G_s	6			0.57	Default value equals that of water
k_{soil}	W m^{-1} K^{-1}	23	heat conductivity of the soil, compute T_{sed}	6	Observations or soil map	default value	2.4	Default value represents global value
Δz_{gw}	m	23	distance to groundwater or deep soil temperature, compute T_{sed}	6			2	Can be used for calibration
z_0	m	16,17	aerodynamic roughness	6	Default value		0.0001-1; 0.02 for grassland	default depends on land cover
z_{0h}	m	16	roughness length for heat	6	Default value		$0.1z_0$	
C_H	-	14	bulk transfer coefficient heat, to compute sensible heat exchange	6	Default value for large water bodies; Equation 16 for small ones		0.0011 (large water bodies)	
C_E	-	15	bulk transfer coefficient water vapour, to compute latent heat exchange	6	Default value for large water bodies; Equation 16 for small ones		0.0011 (large water bodies)	
F_{dr}	m s^{-1}	26	flow of water entering the water body laterally (surface runoff, drainage,..)	6	TOXSWA			
T_{dr}	K	26	compute lateral heat input	6	Soil temperature at drain depth			Time series

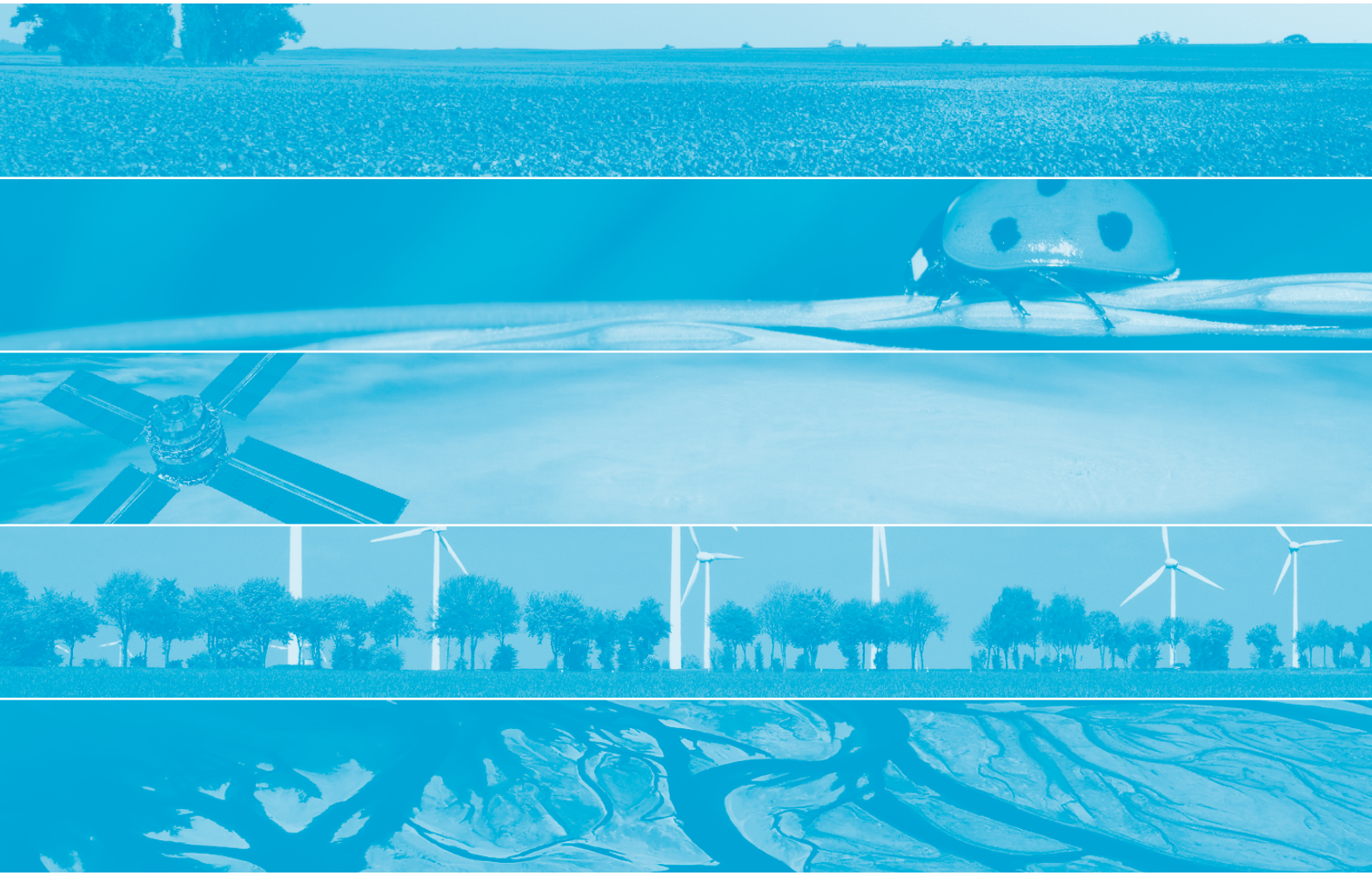

Alterra is part of the international expertise organisation Wageningen UR (University & Research centre). Our mission is 'To explore the potential of nature to improve the quality of life'. Within Wageningen UR, nine research institutes – both specialised and applied – have joined forces with Wageningen University and Van Hall Larenstein University of Applied Sciences to help answer the most important questions in the domain of healthy food and living environment. With approximately 40 locations (in the Netherlands, Brazil and China), 6,500 members of staff and 10,000 students, Wageningen UR is one of the leading organisations in its domain worldwide. The integral approach to problems and the cooperation between the exact sciences and the technological and social disciplines are at the heart of the Wageningen Approach.

Alterra is the research institute for our green living environment. We offer a combination of practical and scientific research in a multitude of disciplines related to the green world around us and the sustainable use of our living environment, such as flora and fauna, soil, water, the environment, geo-information and remote sensing, landscape and spatial planning, man and society.

More information: www.alterra.wur.nl/uk